5. ORIGIN AND THERMAL EVOLUTION OF MARS

G. SCHUBERT
University of California, Los Angeles

S. C. SOLOMON
Massachusetts Institute of Technology

D. L. TURCOTTE
Cornell University

M. J. DRAKE
University of Arizona

and

N. H. SLEEP
Stanford University

The thermal evolution of Mars is governed by subsolidus mantle convection beneath a thick lithosphere. Models of the interior evolution are developed by parameterizing mantle convective heat transport in terms of mantle viscosity, the superadiabatic temperature rise across the mantle and mantle heat production. Geological, geophysical and geochemical observations of the composition and structure of the interior and of the timing of major events in Martian evolution, such as global differentiation, atmospheric outgassing and the formation of the hemispherical dichotomy and Tharsis, are used to constrain the model computations. Isotope systematics of SNC meteorites suggest core formation essentially contemporaneously with the completion of accretion. Ancient fluvial landforms and a high atmospheric D/H ratio imply substantial degassing and

atmosphere formation early in the history of Mars. Accretional considerations also favor initial melting of much of the outer portions of the planet. Initial conditions assumed for the thermal history calculations thus include full differentiation of a silicate mantle and metal-sulfide core and a mantle at a high, near-solidus temperature. The subsequent thermal evolution involves cooling of the mantle and core, differentiation of a crust and thickening of a rigid lithosphere. As a result of the removal of much of the initial interior heat by vigorous mantle convection, perhaps augmented by an upward concentration of heat-producing elements into the crust, the rate of decrease of mantle temperature and surface heat flow was much more rapid during the first 1 Gyr of Martian history than subsequent to that era. Crustal production rates were also much higher in the first 1 Gyr of Martian evolution than later in the planet's history. This temporal behavior is consistent with geologic evidence for a general decrease with time in the Martian volcanic flux and, following a brief initial period of massive crustal formation, early global contraction recorded in the widespread formation of wrinkle ridges on geologically ancient surface units. The thermal evolution models predict a present lithosphere thickness several 100 km thick, in agreement with estimates of elastic lithosphere thickness inferred from the response to major surface loads. Numerical calculations of fully three-dimensional, spherical convection in a shell the size of the Martian mantle are carried out to explore plausible patterns of Martian mantle convection and to relate convective features, such as plumes, to surface features, such as Tharsis. The models have upwellings in the form of interconnected sheets. There is no single dominant plume. Therefore, if Tharsis is associated with one or more mantle plumes, then the lithosphere beneath Tharsis must be thinned or cracked either to promote plume concentration in the region or to facilitate magma migration through the lithosphere. Thermal history models for Mars admit present core states similar to the Earth, but they also allow completely fluid cores and cores closer to complete freezing. The key parameter distinguishing among these possibilities is the weight fraction of sulfur in the core. If this fraction is ~ 15% or more, then the present Martian core is completely fluid and there is no thermal convective dynamo. The unambiguous determination of the presence or absence of an intrinsic Martian magnetic field by future spacecraft missions will provide an essential constrain on interior structure and thermal evolution models. The eventual measurement of the natural magnetic remanence of rock samples on Mars with ages > 3.5 Gyr will also provide an essential test of thermal history and core dynamo models.

I. INTRODUCTION

The acceptance of Mars as the parent body of the SNC meteorites (McSween 1984; Bogard et al. 1984; Becker and Pepin 1984; chapter 4) has profoundly changed our view of the planet's evolution. Martian thermal history models of the late 1970s and early 1980s were largely dominated by the idea that the core of Mars formed subsequent to its accretion, after radioactive heating had raised the temperatures in the planet's interior sufficiently above the relatively cold initial temperatures to initiate melting and gravitational separation of Fe-FeS (Johnston et al. 1974; Solomon and Chaiken 1976; Johnston and Toksöz 1977; Toksöz et al. 1978;

Toksöz and Hsui 1978; Solomon 1978,1979; Arvidson et al. 1980; Davies and Arvidson 1981). Core formation in these models occurred as late as a few Gyr after Mars accreted, and the segregation of the core lasted for up to 1 Gyr. Late core formation was supported by the notion that Martian surface geology was dominated by extensional tectonics, requiring global heating and planetary expansion until late in the planet's evolution (Solomon and Chaiken 1976; Solomon 1978,1979). However, the U/Pb isotopic composition of SNC meteorites requires core formation at about 4.6 Gyr ago (Chen and Wasserburg 1986), either contemporaneous with accretion or within a few 100 Myr of the end of accretion. We must therefore abandon thermal evolution scenarios of Mars with cold initial temperatures and late core formation and instead adopt the view that accretional heating raised temperatures inside Mars sufficiently high that the core formed early, prior to the end of accretion or within a few 100 Myr thereof, and that Mars began its post-accretional evolution fully differentiated and hot. In this new view of Martian thermal history, early Mars was similar to the larger terrestrial planets Venus and Earth, whose cores formed early as a consequence of high accretional temperatures (see, e.g., Kaula 1979b; Wetherill 1985). The post-accretional evolution of Mars, like that of Venus and Earth, is one of secular cooling.

In the following, we discuss the case for a hot initial Mars and early core formation in greater detail. Numerous lines of evidence, in addition to the U-Pb isotopic composition of SNC meteorites, support an early hot, differentiated planet. The structure of the Martian interior is a major factor in determining the post-accretional thermal history of Mars, and we briefly discuss interior structural models inferred from geophysical and geochemical data (see also chapter 7). In accordance with the model of early core and crust formation, we assume that the major radial structure of Mars has been little changed since the end of accretion (except for the lithosphere, which has thickened with time).

The principal characteristics of Mars, i.e., the north-south crustal dichotomy, the Tharsis Rise, the center of mass-center of figure offset, global tectonic patterns and the possible absence of a magnetic field, must all be understood in terms of the thermal history, and we discuss how these characteristics might be accommodated in a model in which Mars steadily cools from a hot, differentiated start. We present quantitative models of Martian cooling history that parameterize heat transport by subsolidus mantle convection. These models allow us to estimate properties of Mars for which no direct measurements presently exist, such as the cooling rate of the planet, its present lithosphere thickness and surface heat flux, and the present extent of inner core solidification. Finally, we use the results of numerical calculations of fully three-dimensional, spherical convection to discuss convective patterns in the Martian mantle. These computations place constraints on possible convective models for the formation of the hemispheric crustal asymmetry and Tharsis.

II. INTERNAL STRUCTURE

Although the seismic experiment on Viking Lander 2 provided no direct information on Mars' internal structure (Anderson et al. 1977; Goins and Lazarewicz 1979; Toksöz 1979), it is likely that Mars is divided into a crust, mantle and core. However, the thicknesses, densities and compositions of these regions are uncertain (see chapter 7).

A. Core

Geophysical and geochemical data constrain the size and composition of the Martian core. The geophysical data include the mean density of Mars (3933 kg m⁻³; Bills and Ferrari 1978) and its dimensionless axial moment of inertia (0.365, according to Reasenberg [1977] and Kaula [1979a]). The dimensionless axial moment of inertia C/MR^2, where C is the principal moment of inertia about the rotation axis, M is the mass of Mars (6.42×10^{23} kg) and R is the radius of Mars (3390 km) is obtained from the inferred value of J_{2H} (the second-degree zonal coefficient in the spherical harmonic representation of the hydrostatic part of the gravitational potential of Mars). To determine C/MR^2 it is necessary first to remove the relatively large nonhydrostatic contribution J_2 to the observed J_2 ($J_2 = J_s + J_{2H}$). Estimation of J_2 is model dependent and, as a result, the axial moment of inertia of Mars is uncertain. According to Reasenberg (1977) and Kaula (1979a), J_s is principally due to Tharsis (see also Binder and Davis 1973). Under the assumption that the nonhydrostatic contributions to the moments of inertia are symmetric about an equatorial axis through the center of Tharsis, it can be shown that $C/MR^2 = 0.365$ (Reasenberg 1977; Kaula 1979a). Bills (1989a) has recently suggested that the nonhydrostatic component of J_2 is more likely to be a maximally triaxial ellipsoid, i.e., with the intermediate moment of inertia exactly midway between the greatest and least moments. This assumption leads to a value of C/MR^2 equal to 0.345. Kaula et al. (1989) have argued that the larger value of C/MR^2 is more physically plausible: (1) because the rotation axis of Mars adjusts sufficiently rapidly compared to changes in nonhydrostatic density anomalies that it is the axis of maximum moment of inertia for the nonhydrostatic density field; (2) because the gravity and topography of Mars are dominated by Tharsis; and (3) because tectonic models of Tharsis require generation and support that are almost axisymmetric about a line from the center of Mars through Tharsis.

Goettel (1981) has explored the consequences of the mean density and moment of inertia I of Mars for the radius of the Martian core and the densities of the planet's core and mantle ($I = (C + B + A)/3$, where A and B are principal moments of inertia about two orthogonal axes in the equatorial plane; $I/MR^2 = C/MR^2 - 2J_2/3; J_2 = 1.96 \times 10^{-3}$). His results, based on $I/MR^2 = 0.365$, are summarized in Table I. (Spherically symmetric compositional models can only be constrained by I/MR^2 and other spherically aver-

TABLE I
Ranges in Properties of the Martian Core Allowed by the Mean Density and Dimensionless Mean Moment of Inertia[a]

Property	Range
Radius	1300–1900 km
Fractional mass	13–26%
Central pressure	45–37 GPa
Density	8900–5800 kg m⁻³

[a] $I/MR^2 = 0.365$ assumed. Table after Goettel 1981.

aged observables.) Mars could possess either a small, iron-rich core of high density (a pure Fe core would have a density of 8090 kg m⁻³ and constitute 14.8% of the mass of Mars), or a large, low-density core with substantial S (or other light element). An FeS core would have a density of 5770 kg m⁻³ and comprise 26.3% of the mass of Mars. The core mass increases with its size despite the density decrease (Fig. 1). Goettel's (1981) results for core properties consistent with the mean density and the mean moment of inertia of Mars are in general agreement with the predictions of other models (Johnston and Toksöz 1977; Okal and Anderson 1978; Basaltic Volcanism Study Project 1981). On the basis of all these models, the probable radius of the Martian core lies in the range 1500 to 2000 km, and the fractional mass of the planet occupied by the core is likely to be between 15 and 30%.

Independent geochemical evidence on the mass of the Martian core is provided by the SNC meteorites. Treiman et al. (1987) have determined the
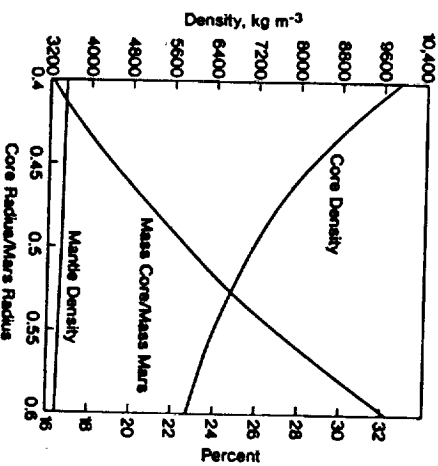

Fig. 1. Core density ρ_c, mantle density ρ_m and fractional core mass vs normalized core radius x for a two-layer model of Mars consistent with the mean density (3393 kg m⁻³) and dimensionless moment of inertia (0.365). The curves are simultaneous solutions of the equations 3933 kg m⁻³ = ρ_m + (ρ_c − ρ_m)x³ and (0.365)(3933)(2.5) kg m⁻³ = ρ_m + (ρ_c − ρ_m)x⁵.

abundances of siderophile and chalcophile elements in the mantle of Mars from SNC meteorite abundances (using an element correlation method); they have modeled these abundances in terms of segregation of metal into the core. The abundances of siderophile and chalcophile elements may be substantially matched if Mars accreted homogeneously and a metallic core constituting 25 to 35 wt% of the planet formed in chemical equilibrium with the mantle. Best fits are achieved if the core material during differentiation consisted of ~ 50% S content of such a core would be ~ 12.5 wt%. The ratio of Fe to Ni is poorly known, and the relative fractions of the solid and liquid components of both the early and modern core are unconstrained.

Laul et al. (1986) have also calculated the mass and composition of the core by assuming C I abundances of Fe and Ni and a 0.35 × C I abundance of S. From mass balance, and abundances of these elements inferred for the Martian mantle from the compositions of the SNC meteorites, they obtained a core comprising 21.7 wt% of the planet, with an S abundance of 14 wt%. Laul et al. (1986) also conclude that Mars accreted homogeneously and that the core is in equilibrium with the mantle. However, the low core mass that they compute does not yield as good a fit to the depletions of siderophile and chalcophile elements as the larger core masses of Treiman et al. (1987).

We will see in Sec.IV.A that the abundance of S in the core of Mars is a crucial parameter determining the extent to which the core solidifies as the planet cools through geologic time. Unfortunately, the S content of the Martian core must still be considered as uncertain. The agreement between the estimates of Laul et al. (1986) and Treiman et al. (1987) of the wt% S in the Martian core, while encouraging, may only reflect the use of the same limited geochemical data set by both groups.

B. Mantle

Consistent with the core properties summarized in Table I, the thickness of the Martian mantle ranges between ~ 1500 and 2100 km. The zero pressure density of the mantle, for I/IMR^2 = 0.365, is between ~ 3400 and 3470 kg m⁻³ (Goettel 1981). If the olivine-spinel phase transition occurs in the Martian mantle, it would be found at depths greater than approximately 1000 km (Basaltic Volcanism Study Project 1981; see chapter 7). Still higher-pressure phase changes involving the formation of perovskite and magnesiowustite might occur in the deep lower mantle of Mars depending on the size of the Martian core (chapter 7).

C. Crust

Mars has a distinct low-density crust of variable thickness, as indicated by the partial to complete isostatic compensation of surface topography (Phillips et al. 1973; Phillips and Saunders 1975). The mean thickness of the crust, however, is poorly constrained. A minimum value for the average crustal

thickness of 28 ± 4 km (depending on choice of crust-mantle density difference) was obtained by Bills and Ferrari (1978) by fitting a model crust of uniform density and variable thickness overlying a uniform mantle to topography and gravity expressed in spherical harmonics to degree and order 10; for this minimum mean thickness, the crust is of zero thickness beneath the Hellas basin. For a crustal thickness of 15 km at the Viking 2 Lander site, a value derived from arrival times of seismic phases of a possible Marsquake interpreted as waves reflected off the crust-mantle boundary (Anderson et al. 1977), Bills and Ferrari (1978) obtained a mean crustal thickness of 37 ± 3 km. The crustal thickness beneath the Hellas basin in this model is 9 ± 1 km while beneath Tharsis it is 69 ± 8 km. In all the models of Bills and Ferrari (1978), maximum crustal thickness occurs beneath Tharsis and minimum crustal thickness is found beneath the Hellas basin. Sjogren and Wimberly (1981) used topography and gravity data to infer that the Hellas basin is isostatistically compensated at a best-fitting compensation depth of 130 ± 30 km. From the models of Bills and Ferrari (1978), this value corresponds to a globally averaged crustal thickness of ~ 150 km.

The approximately hemispherical division of the Martian surface between the topographically lower and stratigraphically younger northern plains and the heavily cratered southern uplands, often termed the crustal dichotomy, is associated with thicker crust in the southern hemisphere (see, e.g., Janle 1983). The hemispheric crustal dichotomy contributes to the Martian center of mass-center of figure offset, as does the Tharsis bulge. The Martian center of figure is displaced from the center of mass by ~ 2.5 km toward a direction approximately midway between the centers of the southern highlands and the Tharsis bulge (see chapter 7).

III. CONSTRAINTS ON THERMAL EVOLUTION

Among the major constraints on thermal history models of Mars is the origin of the present internal structure of the planet. Viable thermal evolution models must account for the timing and formation of the core, the hemispheric crustal dichotomy, and the Tharsis Rise. Models should provide an explanation for the lack of magnetic field at present, or, if future observations should prove the existence of a small Martian magnetic field, the models should allow for the generation of that field. Thermal history models should be consistent with the evolution of surface stresses and strains as revealed by global tectonic patterns.

A. Core Formation

U-Pb data for several SNC meteorites intercept the concordia curve at about 4.5 Gyr as well as at a younger age variously thought to represent the crystallization age of the shergottites (Jones 1986) or the impact event that resulted in ejection of SNC material from the parent body (Chen and Wasser-

burg 1986). The 4.5 Gyr "age" indicated by U-Pb data, as well as whole-rock Rb-Sr model ages for SNC meteorites of about 4.6 Gyr (Shih et al. 1982), suggest early global differentiation, including formation of the core essentially contemporaneously with the completion of accretion. Differentiation of a core would mean on average by as much as 300 K (Solomon 1979). A hot initial state for the planet is indicated by these results. Other indicators of a hot early Mars include: (1) the old age (≥4 Gyr) of the southern hemisphere highlands, suggesting early crustal differentiation (see below). The interpretation of D/H in terms of early loss of water is not unique. Yung et al. (1988) and Jakosky (1990a) suggest loss of water over geologic time, while Zahnle et al. (1990a) argue for loss of water upon accretion.

Early core formation is made possible by the high accretional temperatures achieved through the burial of heat by large impacts (Kaula 1979b; Wetherill 1985). An example of accretional temperature profiles for Mars is shown in Fig. 2 (Coradini et al. 1983). In this example, there is a power-law distribution of impacting planetesimals by size, 30% of the impact kinetic energy is retained as heat, and a 100-Myr time scale of accretion is assumed. For this particular model, melting of a 360-km-thick shell occurs at the end of accretion. Models with higher temperatures and larger degrees of melting
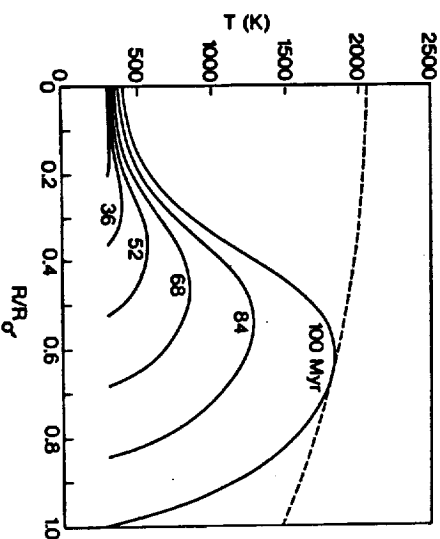

T (K)

Fig. 2. Model accretional temperature profiles for Mars (figure after Coradini et al. 1983). The calculations are based on a 100 Myr accretion time scale and the assumption that 30% of the impact kinetic energy is retained as heat in the growing planet. The dashed curve is a model solidus temperature profile.

are possible, for example, by adoption of a larger value for the percent of impact kinetic energy retained as heat.

The importance of large impacts in the formation of the terrestrial planets and the validity of the 100-Myr accretional time scale are demonstrated by the planetary accumulation models of Wetherill (1985,1986). The spin and orbital properties of Mars and the other planets, especially their obliquities, are plausibly explained as consequences of impacts with large bodies during the process of planetary formation (Harris and Ward 1982; Hartmann and Vail 1986). A major problem in understanding the growth of Mars according to present models of planetary accretion is that the calculations typically result in objects that are several times more massive than Mars (Wetherill 1985,1986). The size of Mars may have been limited by disturbances to the planetesimal source population for Mars associated with outer-planet secular resonance regions, assuming of course that the formation of the outer planets preceded the growth of Mars (Wetherill 1986).

B. Magnetic Field

Mars may have a weak magnetic field, though this hypothesis is presently a matter of dispute (Russell et al. 1984; Dolginov 1987; see chapter 31). A fit of a dipole to the available Soviet magnetic field data gives a moment of 2×10^{12} Tesla-m^3 (2×10^{22} gauss-cm^3), or 3×10^{-4} times the Earth's moment, tilted ~ 15° with respect to the rotation axis and oriented in the opposite sense to the Earth's dipole moment (Dolginov et al. 1973,1976). A re-evaluation by Russell (1978b) leads only to an upper bound on the moment of 2×10^{11} Tesla-m^3, an order of magnitude less than the value of Dolginov and co-workers. Recent Phobos observations of the Martian magnetotail give no indication of an intrinsic planetary magnetic field (Riedler et al. 1989b; Ong et al. 1989). Magnetic field measurements in the close vicinity of Mars are needed to resolve this issue.

Several SNC meteorites display natural remanent magnetization (NRM) consistent with a magnetizing field of less than ~ 8 A/m (0.1 oe; Cisowski 1986). The timing and acquisition mechanism of the NRM are not well established, but it has been inferred that the magnetizing event was shock metamorphism during impact (Cisowski 1986). Whether an internal magnetic field on Mars is indicated at the time the SNC meteorites were ejected from the planet is unclear.

C. Crustal Dichotomy

The relative chronology of the various large-scale surface units on Mars is reasonably well established from stratigraphic and crater density relationships (see, e.g., Carr et al. 1973; Tanaka et al. 1988; also see chapters 11 and 12). The oldest units are the cratered terrain, an upland region as heavily cratered as the lunar highlands and occupying approximately the hemisphere south of a great circle inclined 35° to the equator (Mutch and Saunders 1976).

While the absolute chronology of the Martian surface is a matter of debate (see, e.g., Hartmann 1973b,1977; Soderblom et al. 1974; Neukum and Wise 1976; Neukum and Hiller 1981; see chapter 12), most workers are in agreement that the heavily cratered southern uplands probably record the terminal phase of heavy bombardment of the inner solar system, dated for the Moon at 3.9 to 4.0 Gyr ago. The bulk of crustal formation must have occurred prior to this time.

The approximately hemispherical dichotomy between the ancient southern highlands and the younger northern plains is generally held to be an ancient first-order feature of the Martian crust. The dichotomy has been ascribed variously to a very long-wavelength mantle convective planform (Lingenfelter and Schubert 1973; Wise et al. 1979a), to post-accretional core formation (Davies and Arvidson 1981), and to a giant impact (Wilhelms and Squyres 1984). In view of the evidence from SNC meteorites discussed above, that core separation occurred essentially contemporaneously with accretion, scenarios for the formation of the crustal dichotomy involving late core-mantle segregation (Wise et al. 1979a; Davies and Arvidson 1981) may be discounted. Whether the dichotomy was the result of endogenic or exogenic processes, however, remains unresolved despite considerable ongoing photogeological analysis of the dichotomy boundary region (see, e.g., McGill 1988; Wilhelms and Baldwin 1989a).

D. Volcanic Flux

Mars shows abundant evidence of surface volcanic activity spanning a wide range of relative geologic ages (see chapter 13). There are numerous volcanic constructs, including the large volcanoes of the Tharsis province, and extensive volcanic plains with apparent flow fronts and other features associated with volcanic units (Carr 1973,1974; Malin 1977; Carr et al. 1977). There are relatively old and relatively young examples of both plains and shields. While the stratigraphic sequence of major volcanic units has been reasonably well established from crater density and superposition relationships (Tanaka et al. 1988), estimates of the absolute ages of volcanic units depend upon knowledge of the scaling of cratering flux and impacting-object size vs crater size from the Moon to Mars, knowledge that is, at best, incomplete (see, e.g., Chapman 1974; Wetherill 1974; Hartmann et al. 1981). Published ages for the stratigraphically young surfaces of the Tharsis shields, for instance, range from 2.5 Gyr (Neukum and Wise 1976) to on the order of 0.1 Gyr (see, e.g., Hartmann 1977).

An important constraint on global thermal evolution is the volcanic flux through time. Estimates of the surface area of volcanic material at each major stratigraphic stage, including corrections for later burial, have been given by Greeley (1987) and Tanaka et al. (1988). Both find 2×10^8 km^2 of volcanic material, though the two analyses differ in detail, particularly in the relative strength of a "peak" in the flux curve at early Hesperian times (corresponding

to the formation of the Martian ridged plains) ~ 3 to 3.5 Gyr ago (Tanaka 1986). In the synthesis of Tanaka et al. (1988), the early Hesperian "peak" is quite modest; a monotonic or nearly monotonic decrease of flux with time is implied. Greeley (1987) has suggested that the volume of volcanic material may be estimated by multiplying the area by an average thickness of ~ 1 km. A volume of 2×10^8 km^3 is equivalent to a global layer of volcanic material 1.5 km thick. Because the volume of igneous intrusions accompanying each eruption is generally larger than the volume of volcanic material (by a factor of 10 in continental regions on Earth [Crisp 1984] and perhaps even larger on Mars), a significant fraction of the Martian crust may have been added by igneous activity since the end of heavy bombardment.

E. Global Tectonic Deformation

Large-scale patterns of tectonic deformation on a planetary surface can be direct signatures of global thermal evolution (see chapter 8). For a planet with a globally continuous lithosphere, such as Mars, warming or cooling of the interior will give rise to net global expansion or contraction and thus, respectively, to extensional or compressional horizontal stress and strain near the planetary surface. The magnitude σ_t of thermal stress accumulated in any time interval is given by

$$\sigma_t = [E/(1 - \nu)]\Delta R/R \qquad (1)$$

where E and ν are the Young's modulus and Poisson's ratio of near-surface material and $\Delta R/R$ is the fractional change in radius during that time interval (Solomon 1986). The fractional radius change is related to the radial distribution of temperature change $\Delta T(r)$ by

$$\Delta R/R = (1/R^2) \int_0^R \alpha(r)\Delta T(r)dr \qquad (2)$$

where α is the volumetric coefficient of thermal expansion. For $\alpha = 3 \times 10^{-5}$K^{-1}, a change ΔT in average interior temperature of 100 K yields $\Delta R/R = 10^{-3}$ or $\Delta R = 3$ km. From Eq. (1), with $E = 80$ GPa and $\nu = 0.25$, such a radius change corresponds to $\sigma_t = 100$ MPa (1 kbar). Sufficiently large thermal stress and strain should be visible in globally distributed tectonic features whose timing and sense of deformation yield strong constraints on the history of internal temperatures (see, e.g., Solomon and Chaiken 1976). Large-scale tectonic features confined to a regional, rather than global, scale are also important indicators of thermal evolution, particularly of the characteristics of heat and strain imparted to the lithosphere by mantle dynamic processes.

The view of Martian tectonics that followed the Mariner 9 mission was that the planet experienced a prolonged period of lithospheric extension which gave rise to the extensive systems of graben mostly centered on the

Tharsis region (Hartmann 1973c; Carr 1974b), the Valles Marineris canyon system (Sharp 1973) and the pervasive volcanism (Carr 1973). Thermal history models consistent with this view of tectonic evolution involved net warming and global expansion over much of the Martian history. The net warming was attributed variously to late core formation (Solomon and Chaiken 1976), to radioactive heating of the mantle following low-temperature differentiation of a sulfur-rich core (Toksöz and Hsui 1978), or to degassing of the interior and a consequent stiffening of the mantle rheology (Tozer 1985). As noted above, a hot initial state is now indicated for Mars from lead isotope data and planetary accretion considerations, so scenarios involving an initially cool interior (see, e.g., Solomon and Chaiken 1976; Toksöz and Hsui 1978) are not viable. Further, thermal history calculations explicitly including interior degassing and the consequent effect on mantle viscosity (McGovern and Schubert 1989) do not show a secular warming of the mantle as suggested by Tozer (1985).

Much of the evidence for lithospheric extension on Mars is provided from tectonic features in and near the Tharsis area. Although the extensional fractures radiating from the center of Tharsis span a region more than 8000 km across, Tharsis may nonetheless be regarded as a regional feature rather than part of a response to global stress. Further, there are important compressional features located in the ridged plains of Tharsis and oriented approximately circumferential to the center of activity (Wise et al. 1979b). Considerable effort has gone into understanding the evolution of the Tharsis province from this regional perspective. The long-wavelength gravity and topography of the region are not consistent with complete isostatic compensation by a single mechanism, such as crustal thickness variations (Phillips and Saunders 1975). Complete local isostasy is possible, however, if a combination of Airy (crustal thickness variations) and Pratt (mantle density variations) mechanisms act in concert; but this is possible only if the crust is relatively thin (or is pervasively intruded by high-density plutonic material) beneath the Tharsis Rise and substantial density anomalies persist to at least 300 to 400 km depth (Sleep and Phillips 1979,1985; Finnerty et al. 1988). Alternatively, a portion of the high topography of Tharsis can be supported by membrane stresses in the elastic lithosphere (Banerdt et al. 1982; Willemann and Turcotte 1982).

These compensation models have been used to predict lithospheric stresses for comparison with the observed distribution of tectonic features. The isostatic model for Tharsis predicts stresses in approximate agreement with the distribution and orientation of extensional fractures in the central Tharsis region and of compressive wrinkle ridges, while the model involving lithospheric support of a topographic load predicts stresses consistent with the more distal extensional features in regions adjacent to the Tharsis Rise (Banerdt et al. 1982; Sleep and Phillips 1985). An evolution in the nature of the support of Tharsis topography has been suggested (Banerdt et al. 1982; Solomon and Head 1982), though the sequence depends upon the relative

ages of distal and proximal tectonic features. If the distal features are older, then viscoelastic relaxation of stresses associated with an early episode of lithospheric loading may have led to an essentially isostatic state at present; if the distal features are younger, then a progression from local isostasy to lithospheric support as the Tharsis Rise was constructed may have been the natural consequence of global interior cooling and lithospheric thickening (Sleep and Phillips 1985). This distinction is complicated by the fact that superimposed global thermal stress is apparently required to account for the formation of many of the graben and wrinkle ridges, particularly in regions where both types of features are present.

Recent work on Martian tectonics may sharpen the constraints on global thermal stress. Chicarro et al. (1985) have utilized Viking images to map the global distribution of wrinkle ridges on Mars, including regions distant from Tharsis. They find that ridges occur commonly throughout ancient terrain. In volcanic plains, however, the distribution is highly uneven, with ridges strongly concentrated in the ridged plains units and in spotty occurrences in other regions. The lower Hesperian age (approximately 3 to 3.5 Gyr ago) for the most major ridged plains units (Tanaka 1986) and the contrast in ridge density between cratered uplands and young volcanic plains (Chicarro et al. 1985) suggest that ridge formation may have been concentrated in a comparatively early state in Martian evolution (Watters and Maxwell 1986). Examining of crosscutting relations between ridges and graben also supports the view that most ridge formation in the Tharsis region was restricted to an early time period (Watters and Maxwell 1983).

The Martian tectonic history most consistent with all of these findings is one in which Tharsis evolved after the end of heavy bombardment from a primarily isostatic state to one with long-term lithospheric support. Super-imposed on the stresses associated with the Tharsis Rise was a globally compressive stress produced by significant interior cooling in the interval 3 to 4 Gyr ago. Any additional cooling (or warming) in the last 3 Gyr has been sufficiently modest so that further changes in planetary volume have not led to widespread development of young compressive (or extensional) features.

F. Lithospheric Thickness

Estimates of lithospheric thickness on Mars provide important constraints on near-surface thermal gradients and thus on heat flux. The thickness of the thermal lithosphere may be inferred approximately from the heights of volcanic constructs, and the thickness of the elastic lithosphere may be inferred from the response to volcanic loads.

Volcanic constructs on Mars show a tendency to increase in height with time of formation, in that the oldest such features are a few kilometers high and the youngest shields are approximately 20 km high with respect to surrounding terrain (Carr 1974b; Blasius and Cutts 1976). This relationship has been ascribed to an increase in the hydrostatic head of the magma with time

because of a progressive deepening of the source region (Vogt 1974; Carr 1976). Assuming a relative density contrast of 10% between magma and average overburden, and ignoring viscous head loss, these heights give depths to magma chambers varying from perhaps as little as a few tens of km to somewhat over 200 km over the history of Martian shield formation.

The thickness T_e of the elastic lithosphere of Mars has been estimated from the tectonic response to individual loads (Thurber and Toksöz 1978; Comer et al. 1985) and from the global response to the long-wavelength load of the Tharsis Rise (Banerdt et al. 1982; Willemann and Turcotte 1982). The spacing of graben circumferential to the major volcanoes Ascraeus Mons, Pavonis Mons, Arsia Mons, Alba Patera and Elysium Mons indicate values for T_e of 20 to 50 km—equivalently, values of flexural rigidity D of 10^{23} to 10^{24} N-m (10^{30} to 10^{31} dyn cm) at the times of graben formation (Comer et al. 1985). For the Isidis basin region, the elastic lithosphere thickness is inferred to have exceeded 120 km ($D > 10^{25}$ N-m) at the time of mascon loading and graben formation (Comer et al. 1985). The absence of circumferential graben around Olympus Mons requires the elastic lithosphere to have been at least 150 km thick ($D > 3 \times 10^{25}$ N-m) at the time of loading (Thurber and Toksöz 1978; Comer et al. 1985; Janle and Jannsen 1986). Models of the response of Mars to the long-wavelength topography of the Tharsis Rise provide a reasonable fit to the geoid and to the distribution of tectonic features in the Tharsis province if the elastic lithosphere of Mars is globally ~ 100 to 400-km thick, corresponding to $D = 10^{25}$ to 7×10^{26} N-m (Banerdt et al. 1982; Willemann and Turcotte 1982).

The values for T_e derived for individual loads are not consistent with a simple progressive increase with time in the thickness of the elastic lithosphere of Mars. The largest estimates of T_e, for instance, are for perhaps the oldest (Isidis mascon) and youngest (Olympus Mons) features considered (Tanaka et al. 1988). Spatial variations in elastic lithosphere thickness must have been at least as important as temporal variations (Comer et al. 1985). In particular, there appears to have been a dichotomy in lithosphere thickness that spanned a significant interval of time, with comparatively thin elastic lithosphere ($T_e = 20$ to 50 km) beneath the central regions of major volcanic provinces and substantially thicker elastic lithosphere (T_e in excess of 100 km) beneath regions more distant from volcanic province centers and appropriate for the planet as a whole.

The values of T_e may be converted to estimates of the lithospheric thermal gradient and heat flow, given a representative strain rate and a flow law for ductile deformation of material in the lower lithosphere and estimates of lithospheric thermal conductivity. Under the assumption that the large values of elastic lithosphere thickness determined from the local response to the Tharsis Isidis mascon and Olympus Mons and from the global response to the Tharsis Rise exceed the thickness of the Martian crust, the depth to the base of the

mechanical lithosphere is determined by the ductile strength of the mantle. The minimum values of T_e for the Isidis mascon and Olympus Mons correspond, by this line of reasoning, to mean lithospheric thermal gradients of no greater than 5 to 6 K km^{-1} and heat flow values < 17 to 24 mW m^{-2} (Solomon and Head 1990). For the Tharsis Montes and Alba Patera, the mechanical lithosphere thickness is likely governed by the strength of crustal material. The mean thermal gradients consistent with the values of T_e for these loads under this assumption fall in the range 10 to 14 K km^{-1} and heat flow values in the range 25 to 35 mW m^{-2} (Solomon and Head 1989). Essentially contemporaneous temperature differences of at least 300 K at 30 to 40 km depth are implied at a late stage in the development of the Tharsis province. Such temperature differences are too large to be solely the effect of large impacts that occurred some Gyr earlier (Bratt et al. 1985), but they are broadly similar to the temperature variations associated with lithospheric reheating beneath hot-spot volcanic centers on Earth (McNutt 1987). The temperature and heat-flow anomalies beneath the central regions of major volcanic provinces on Mars are presumably also related to mantle dynamic processes, such as convective upwelling plumes and magmatism. Lithospheric thinning beneath the central regions of major volcanic provinces by hot, upwelling mantle plumes can account for the different estimates of elastic lithosphere thickness in these regions as compared with the global average.

G. Mantle Heat Sources

Of particular importance to the thermal evolution of Mars are the concentrations of the radiogenic heat-producing elements K, Th and U in the Martian mantle. Estimates of the abundances of these elements have been made by Taylor (1986), Treiman et al. (1986) and Laul et al. (1986) using SNC meteorites. Taylor (1986) plots analyses of the meteorites on a K/U vs K diagram and shows that the SNC meteorite data are consistent with terrestrial data. The K/U ratio in Mars is not distinguishable from the Earth's, but this analysis does not yield information on the bulk K abundance in Mars.

Treiman et al. (1986) and Laul et al. (1986) have estimated abundances of K, Th and U using their correlation with other refractory lithophile elements. The database used by the two sets of authors is substantially the same. Correlations of K with La show that the mantle of Mars has a K/La ratio of ~ 0.3 of the C I ratio. The corresponding Th/La and U/La ratios are ~ 1.7 and 2 times the C I ratio, respectively (Treiman et al. 1986). Uncertainties in each estimate are factors of 2, 1.7 and 2, respectively. The abundances of K, Th and U, assuming that the Martian mantle has C I abundances of La, are summarized in Table II. If the Martian mantle has higher abundances of La, the abundance of K, Th and U must be scaled upward accordingly. The bulk Martian abundances must be reduced in proportion to the mass of the core, assuming that these elements are excluded from the core. The ratios of K/U

TABLE II

Radiogenic Element Abundance Estimates for the Mantles of Mars and Earth

	K (ppm)	Th (ppb)	U (ppb)	K/U	Th/U
Mars[a]	170	48	16	10^4	3
Mars[b]	315	56	16	2×10^4	3.5
Earth[c]	257	102.8	25.7	10^4	4

[a]Treiman et al. 1986.
[b]Laul et al. 1986.
[c]Turcotte and Schubert 1982.

and Th/U are $\sim 10^4$ and 3, respectively, the former being indistinguishable from the Earth's ratio while the latter is lower than the terrestrial value of ~ 4. There is uncertainty in each ratio of about a factor of 2 based on the scatter in the raw data and the lack of knowledge of the absolute values of refractory-element abundances such as La in Mars relative to C I chondrites. Given the uncertainties in these values, we conclude that radiogenic element abundances in the mantles of Mars and Earth are broadly similar.

IV. THERMAL HISTORY MODELS

On the basis of the constraints discussed in the previous section, we present quantitative simulations of Martian thermal history. In its initial state, Mars is hot and completely differentiated into a core and mantle. The mantle temperature is essentially at the solidus and the core is superliquidus. Radiogenic heat sources are assumed to be distributed uniformly through the mantle, although upward concentration of radioactive elements could accompany differentiation of an early crust. The subsequent evolution consists of a simple cooling, with monotonic decreases in temperature, heat flux and convective vigor and a monotonic increase in the viscosity of the mantle. We parameterize convective heat transport through the mantle by a simple Nusselt number-Rayleigh number relationship. The parameterization approach is well established as a way of investigating the thermal evolution of the planets (see, e.g., Schubert et al. 1979; Sharpe and Peltier 1979; Stevenson and Turner 1979; Cook and Turcotte 1981). We employ two different parameterization schemes. With the parameterization model of Stevenson et al. (1983) we focus on the cooling of the core, the extent of core solidification and the generation of a planetary magnetic field by a core dynamo. With the parameterization model of Turcotte et al. (1979), we emphasize crustal differentiation.

A. Coupled Core-Mantle Evolution

The planetary thermal history model of Stevenson et al. (1983) is employed in this section to study the consequences of core cooling for the thermal and physical state of the Martian core and the generation of a magnetic field by thermal or chemical compositional convection in the core. The model includes: (1) mantle radiogenic heat production; (2) a mantle viscosity directly proportional to $\exp(H/RT)$, where H is a constant activation enthalpy, T is a mantle temperature and R is the gas constant; (3) heat transfer by wholemantle subsolidus convection parameterized by a Nusselt number-Rayleigh number relation; (4) coupled energy balance equations for the mantle and core; (5) possible inner core freezeout with exclusion of a light-alloying element (most likely sulfur) which then mixes uniformly through the outer core; and (6) realistic pressure- and composition-dependent freezing curves for the core. More detailed information about the model equations and parameter values can be found in Stevenson et al. (1983) and Schubert and Spohn (1990), who have recently extended the Mars model to include lithospheric growth and the magnetic dipole moment. The solutions we discuss below are actually new calculations, based on the Mars model of Schubert and Spohn (1990), of cases that are almost identical to ones presented in Stevenson et al. (1983). Parameter values are given in Stevenson et al. (1983) and Schubert and Spohn (1990).

Model cooling histories of Mars are typified by the results in Fig. 3, which shows mantle heat flow vs time for models with initial core sulfur concentrations x_s of 10 and 25 wt% (sulfur is assumed to be the light-alloying element in the core in these models). The models with $x_s = 10\%$ and 25%
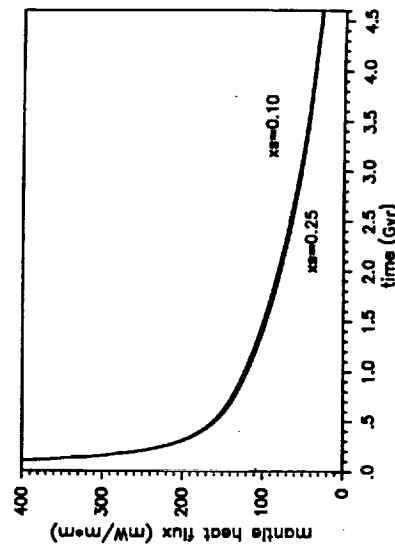

Fig. 3. Heat flow from the mantle vs time for two models of Martian thermal history. Details of the models are given in Stevenson et al. (1983). The models have initial core sulfur concentrations x_s of 10 and 25 wt%, respectively.

are essentially identical to models M1 and M2, respectively, of Stevenson et al. (1983). During the first few 100 Myr of evolution, when the planet is hot and its mantle is convecting particularly vigorously, there is a dramatic decrease in heat flow. Following this early period of rapid cooling is a phase of gradual, slow cooling lasting most of the geologic life of the planet. The present heat flow in these models is ~ 30 mW m^{-2}.

The decrease of mantle temperature with time in these models (Fig. 4) occurs, like the mantle heat flow, in an early period of short and dramatic temperature reduction followed by a decrease of only 200 to 300 K over the last 4 Gyr of the planet's history. The lithospheres in these models grow to thicknesses of ~ 100 km at the present (Fig. 5). Lithosphere thickness and mantle heat flow and temperature are largely independent of the sulfur concentration in the core. The models have thermal boundary layers at the base of the mantle that at present are ~ 100 km thick. Relatively small temperature increases across these bottom boundary layers raise the present core-mantle boundary temperatures of the models ~ 100 K above the mantle temperatures.

The present lithosphere thicknesses in the models of Fig. 5 are smaller, by perhaps a factor of 2 or more, than what would be expected based on our discussion of lithospheric thickness in the previous section. The lithosphere thickness calculated in the models is the thickness of the rheological lithosphere. It is assumed in the models of Fig. 5 that a temperature of 1073 K marks the base of this rheological lithosphere. At temperatures higher than 1073 K, the Martian mantle is taken to be readily deformable on a geologic time scale. Lithosphere thickness is strongly dependent on the concentration of radiogenic heat sources in the mantle. If the mantle heat-source density were half the value assumed in the models of Fig. 5, consistent with the
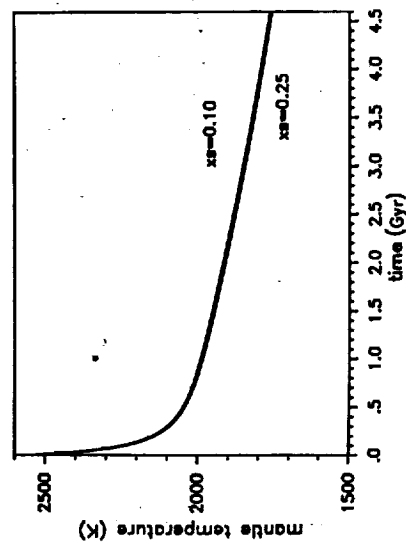
estimates of mantle heat-source densities from SNC meteorite data (refer to our discussion in the previous section), then the present lithosphere thickness would be about 200 km (Spohn 1990). Lithosphere thickness would also be increased by magmatic heat transfer (Spohn 1990) and by upward differentiation of radiogenic heat sources from the mantle into the crust. Thermal history models discussed later in this chapter (Sec. IV.B) demonstrate that depletion of mantle heat sources with time as a consequence of crustal differentiation results in a thicker lithosphere at present. The present lithosphere thicknesses calculated in the models of Schubert et al. (1979) are representative of maximum thicknesses as those models contained no mantle heat sources.

The decrease with time in the heat flow from the core is shown in Fig. 6.

Fig. 5. Thickening of the Martian lithosphere with time in the cooling models of Fig. 3.

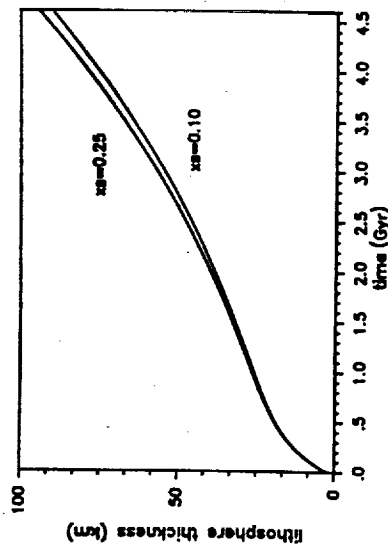Fig. 4. The decrease of characteristic mantle temperature with time in the Martian thermal history models of Fig. 3.
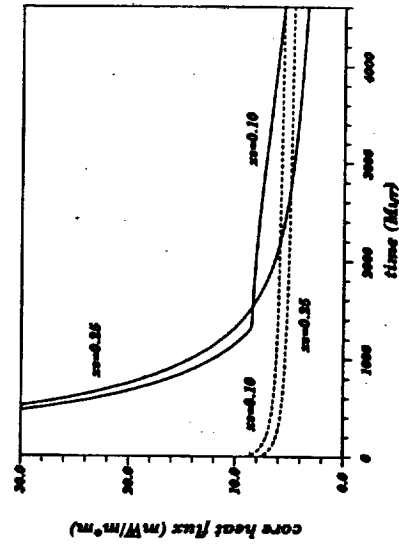
Fig. 6. Core heat flux as a function of time in the Martian thermal evolution models of Fig. 3. The dashed line marks the conductive heat flux along an adiabat in the liquid outer core. The sharp bend in the curve for the model with $x_s = 0.10$ denotes the onset of inner-core solidification.
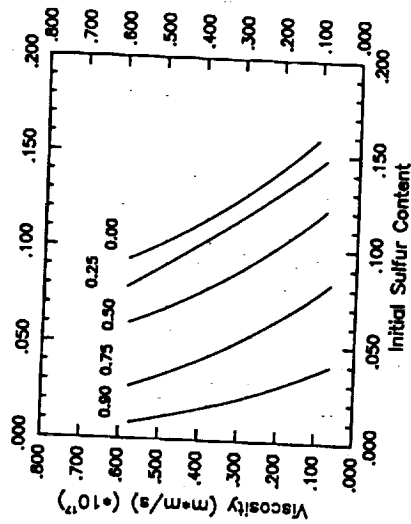
Fig. 7. Contours of fractional inner-core radius as a function of present mantle kinematic viscosity and initial weight fraction sulfur in the core (figure after Schubert and Spohn 1990).
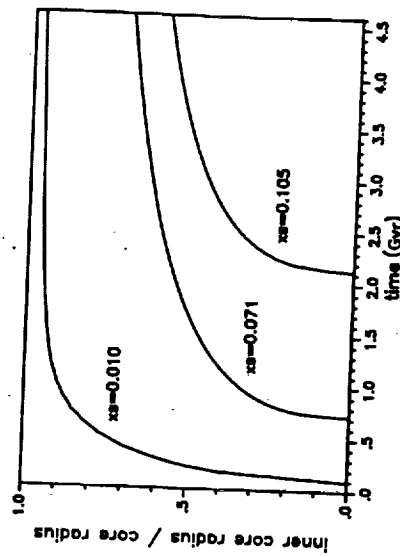

Fig. 8. Fractional inner-core radius vs time for model cooling histories of Mars with three different initial sulfur concentrations x_s in the core (figure after Schubert and Spohn 1990).

for models with x_s = 10% and 25%. Inner-core growth in the x_s = 10% model is marked by the sudden change in the rate of core cooling at ~ 1.3 Gyr after core cooling begins. After 4.5 Gyr, the inner core in this model is about 920 km in radius, leaving an outer liquid core ~ 670-km thick. When inner-core growth in this model begins, the core heat flow is above the estimated value of heat flow conducted along the core adiabat (the upper dashed curve in Fig. 6). Convection in the outer core after ~ 1.3 Gyr is maintained by both thermal and chemical buoyancy, the latter arising from the release of gravitational potential energy upon concentration of the light-alloying element into the outer core. The slow decline in core heat flow after ~ 1.3 Gyr is mainly a consequence of latent heat and gravitational energy release upon inner-core growth. Core heat flow in the x_s = 10% model falls below the heat flow conducted along the adiabat just after 4.5 Gyr. Core convection beyond 4.5 Gyr would still occur but it would be driven entirely by compositional buoyancy. Thermal convective transport after 4.5 Gyr would actually be downward in the core, but the compositional buoyancy would be adequate to offset the slightly stable thermal state. In the x_s = 10% model, a magnetic field would be generated by thermal convection prior to inner core solidification at ~ 1.3 Gyr. Both thermal and chemical convection would support a dynamo for times between 1.3 and 4.5 Gyr. Subsequent to 4.5 Gyr, a magnetic field would be produced by compositionally driven convection associated with inner-core growth.

The sulfur-rich model (x_s = 25%) does not nucleate an inner core. Thermal convection ceases in this model after ~ 2.7 Gyr, when the core heat flux falls below the heat flux conducted along the core adiabat (lower dashed curve in Fig. 6). There is no dynamo action in the core or planetary magnetic field subsequent to 2.7 Gyr. Stevenson et al. (1983) have used the results of the model calculation with x_s = 25% to estimate the smallest initial sulfur fraction for which no inner-core freezeout would occur after 4.5 Gyr; they obtain a value of ~ 15 wt% S.

Schubert and Spohn (1990) have carried out a number of additional Martian thermal history calculations with a view toward more carefully delineating conditions for no inner-core freezeout. Their results are shown in Fig. 7, which gives the dependence of present inner-core radius (as a fraction of total core radius) on both present mantle viscosity and initial wt% sulfur x_s in the core. Present inner-core radius increases with decreasing x_s or decreasing present mantle viscosity because the former increases the core melting temperature and cooling is more rapid with the latter; both result in earlier inner-core freezeout and a longer period of inner-core growth. Fifteen wt% is a good estimate of the minimum core sulfur concentration required for no core freezing through geologic time, unless the present mantle viscosity is ≲ 10^{16} m² s⁻¹ (or ~ 3.5 × 10^{19} Pa s for a mantle density of 3500 kg m⁻³).

Figure 8, after Schubert and Spohn (1990), shows inner-core radius vs time for three different initial S concentrations. Inner-core growth is very

rapid once freezeout begins; the inner core is almost completely grown within 0.5 to 1 Gyr of initial freezeout. The depression of the melting temperature in the outer core as the sulfur concentrates there with progressive inner-core growth and the slowing of the cooling rate as the planet evolves both contribute to the reduction in inner-core growth rate with time. With increasing x_s, the time of initial core freezeout is delayed and the present inner-core radius decreases.

If the estimates of Laul et al. (1986) and Trieman et al. (1987) of 14 and 12.5 wt% S in the Martian core are taken to imply that x_s is ≲ 15 wt%, then

based on Fig. 7, it is likely that Mars has a solid inner core. If Mars has no magnetic field, the explanation may then lie in the nearly complete solidification of the core (Young and Schubert 1974). On the other hand, if the Laul et al. (1986) and Treiman et al. (1987) predictions of wt% S in the Martian core are underestimates, then according to Fig. 7, Mars would not have a solid inner core at present, and the explanation for lack of a present Martian magnetic field might lie in the absence of a drive (a growing inner core) for chemical convection in a core that had cooled too far to convect thermally at present (Stevenson et al. 1983). Our knowledge of Mars is inadequate to distinguish unambiguously between these alternative possibilities, although complete freezing of the Martian core probably requires an unreasonably low content of S in the core. The thermal history models are also consistent with a Mars that presently has a growing solid inner core, a dynamo in its liquid outer core driven by chemical compositional convection, and a planetary magnetic field, albeit a small one. Figure 7 shows that if x_s is ≤ 15 wt%, but not too small, then the core of Mars would only be partially solidified at present and a Martian dynamo and magnetic field would be likely.

This is illustrated in Fig. 9, which shows the results of a model calculation of the Martian magnetic dipole moment μ_M, normalized with respect to the Earth's present magnetic dipole moment, as a function of time for the Mars model with $x_s = 10\%$ and 25%. The calculation of μ_M follows Stevenson et al. (1983) and Schubert and Spohn (1990). The magnetic dipole moment decreases rapidly during the first several 100 Myr of evolution concomitant with the early rapid cooling of the planet and the rapid decline in core heat flow. With $x_s = 10\%$, dynamo action occurs throughout the planet's evolution. Prior to 1.3 Gyr, the model Martian dynamo is driven by thermal convection in the core. There is a sudden increase in μ_M at ∼ 1.25 Gyr coin-

cident with inner-core formation. Subsequent to 1.3 Gyr, the dynamo is driven by both thermal and chemical compositional convection as the inner core solidifies and releases latent heat and gravitational potential energy. With $x_s = 25\%$, there is no inner-core solidification and the dynamo is driven solely by thermal convection until about $t = 2.7$ Gyr when dynamo action ceases because the core heat flux falls below the conductive heat flux along the core adiabat and thermal convection can no longer occur in the core. There is no present magnetic field in this model of Martian evolution because thermal convection is not possible in the present liquid core and there is no source of chemical convection in the core. Because of the uncertainty in the exact value of the conductive heat flux along the Martian core adiabat (Schubert and Spohn 1990), we cannot exclude the possibility that at present there is a weakly thermally convecting liquid core in Mars and a weak dynamo. If it should be determined that Mars has a small magnetic field, then such a model would provide a plausible explanation.

B. Crustal Differentiation

Magmatism in planetary interiors results in crustal formation and the removal of heat-producing radiogenic elements from the planetary mantle. The removal of heat sources reduces the vigor of mantle convection, allows the mantle to cool more rapidly, increases the lithosphere thickness, and reduces surface volcanism. In this section we provide quantitative estimates of the rate of crustal magmatism by extending the approach of Turcotte et al. (1979,1980) to the parameterization of convective cooling in the mantle of Mars. We refer the reader to Turcotte and Huang (1990) for the details of this approach and discuss here only the modifications necessary to simulate crustal production and the depletion of the mantle in radiogenic heat sources. A recent study of Martian thermal history with crustal differentiation has also been carried out by Spohn (1990).

In order to model the loss of heat-producing elements from the interior of Mars to its crust by magma transport, we take the rate of internal heat generation per unit mass H to be given by

$$\frac{dH}{dt} = -H\left(\lambda + \frac{\chi u}{R}\right) \tag{3}$$

where t is time, λ is the radioactive decay rate (2.77×10^{-10}yr^{-1}; Turcotte and Schubert 1982), u is a mean convective velocity in the mantle, R is the radius of Mars and χ is a crustal fractionation parameter. The parameter χ is the ratio of the characteristic turnover time for mantle convection to the characteristic time for crustal fractionation. Based on the present rate of formation of the oceanic crust on the Earth, we show below that $\chi = 0.01$ for the Earth. Of course, the crustal fractionation model developed here is not applicable to the Earth because crustal recycling through subduction is occurring.
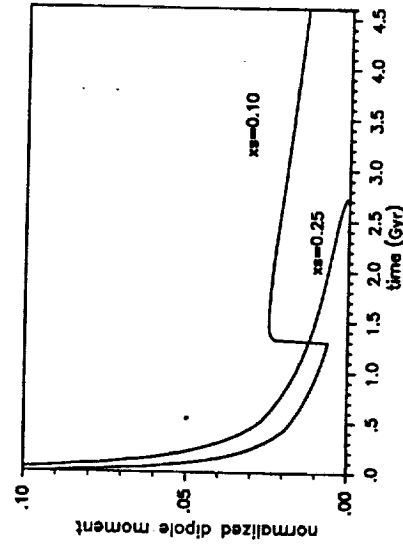

Fig. 9. Normalized magnetic dipole moment vs time for the models of Fig. 3. The dipole moment is normalized with respect to the value of the Earth's present magnetic dipole moment computed following the method presented in Schubert and Spohn (1990).

If the crustal fractionation parameter is sufficiently large then the planet will be fully differentiated. If f is the fraction of crustal material available, then the maximum thickness of crust D_{co} that can be formed is

$$D_{co} = \frac{f \rho_m R}{3 \rho_c}$$ (4)

In deriving Eq. (4) we have neglected the volume of the core. With $f = 0.1$, mantle density ρ_m = 3940 kg m⁻³, crustal density ρ_c = 2900 kg m⁻³ and R = 3398 km, we find that D_{co} = 154 km. The thickness of the evolving crust is assumed to be given by

$$D_c = D_{co}\left(1 - \frac{H}{H_s}\right)$$ (5)

where H_s is the rate of heat generation in the interior without any crustal extraction given by

$$H_s = H_o e^{-\lambda t}$$ (6)

and H_o = 2.47 × 10⁻¹¹ W kg⁻¹ (based on estimates for the Earth; Turcotte and Schubert 1982).

Removal of radioactive elements from the mantle through crustal differentiation affects the growth of the lithosphere by reducing the heat flux from the mantle that must be conducted across the lithosphere. We assume that the heat-producing elements in the crust are sufficiently near the surface that they do not influence the conductive gradient; the base of the lithosphere is defined to lie at a temperature T_r. With these assumptions, the thickness of the conductive lithosphere is given by

$$D_L = (T_r - T_s)\left[\frac{R}{3}\left(\frac{\rho_m H}{k} - \frac{1}{\kappa}\frac{dT}{dt}\right)\right]^{-1}$$ (7)

where k is the thermal conductivity, κ is the thermal diffusivity, T is the mean mantle temperature, and T_s is the surface temperature. The denominator is related to the heat flow through the lithosphere.

The volumetric rate $\dot{V}_v$ of addition of magma to the crust can be determined through its relation to the change in crustal thickness by

$$\dot{V}_v = 4\pi R^2 \frac{dD_c}{dt}$$ (8)

The parameterized convection calculations can also be used to determine whether the radius of the planetary body is increasing or decreasing. The appropriate relation is

$$\frac{\delta R}{R} = -\frac{\alpha}{3}\left[T_o - T\left(1 - \frac{3}{2}\frac{D_L}{R}\right)\right] + \frac{\Delta\rho D_c}{3\rho_m D_{co}}$$ (9)

where T_o is the initial temperature of the planet, α is the volumetric coefficient of thermal expansion and $\Delta\rho$ is the decrease in density associated with crustal differentiation. The first term on the right of Eq. (9) follows from Eq. (2) and the second term represents the increase in volume associated with crustal formation.

We present results of planetary evolution calculations for the following parameter values: κ = 10⁻⁶ m² s⁻¹, thermal conductivity k = 4 W m⁻¹ K⁻¹, T_o = 1000 K, T_s = 255 K, T_r = 2000 K, α = 3 × 10⁻⁵ K⁻¹ and $\Delta\rho$ = 80 kg m⁻³. The mean mantle temperature, crustal thickness, rate of volcanism, lithosphere thickness, surface heat flow and fractional radius change are given in Figs. 10 through 15 as functions of time for various values of the crustal fractionation parameter χ in the range 0 to 10⁻².

The extraction of heat-producing elements into the crust can have important effects on the thermal evolution of Mars. The results for the mean mantle temperature given in Fig. 10 show a temperature reduction of about 250 K if the heat producing elements are removed. It is seen from Fig. 11
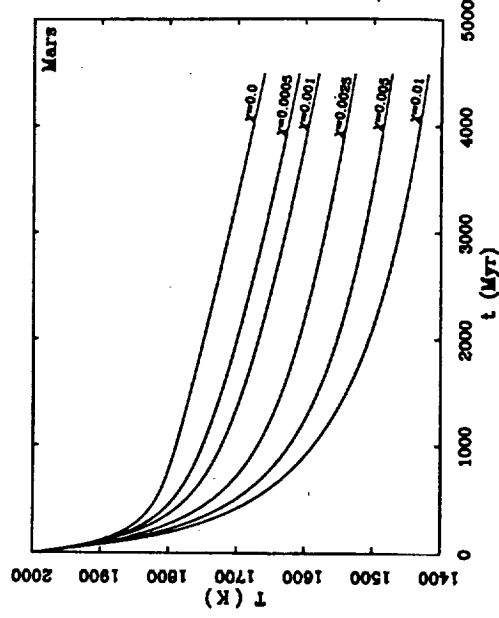

Fig. 10. Dependence of the mean mantle temperature T on time t for several values of the crustal fractionation parameter χ. See text for a discussion of the model used.
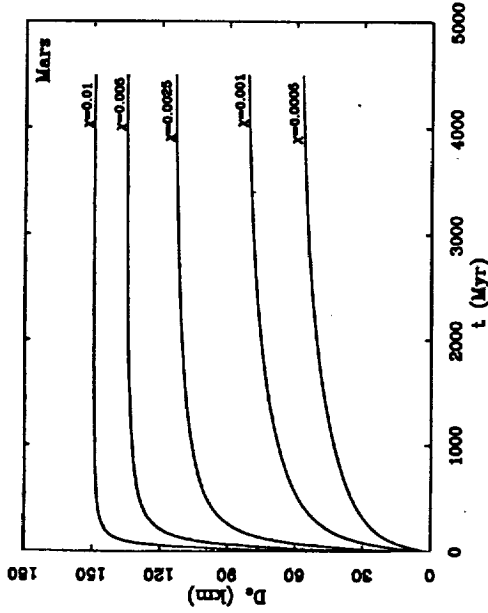
Fig. 11. Thickness of the crust D_c vs time t for a number of values of the crustal fractionation parameter χ. The crustal thickness for a fully differentiated Mars is $D_{cu} = 154$ km.
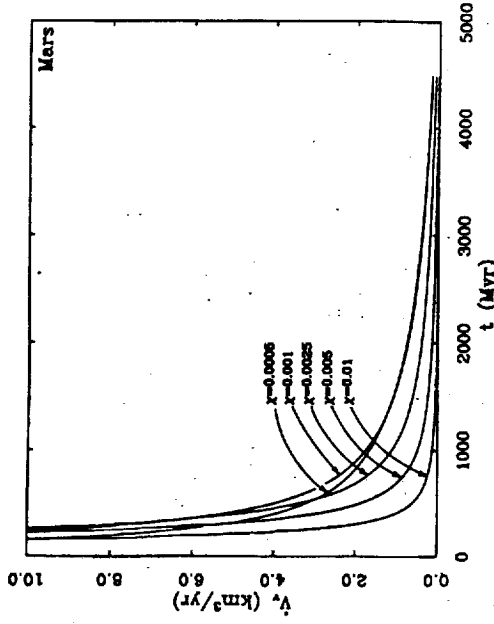

Fig. 12. Dependence of the volumetric flux of Martian volcanism $\dot{V}_v$ on time t for several values of the crustal fractionation parameter χ.
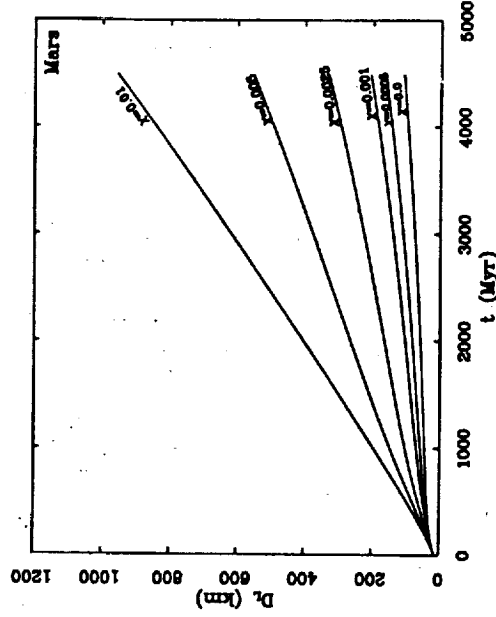

Fig. 13. Thickness of the Martian lithosphere D_L vs time t for several values of the crustal fractionation parameter χ.
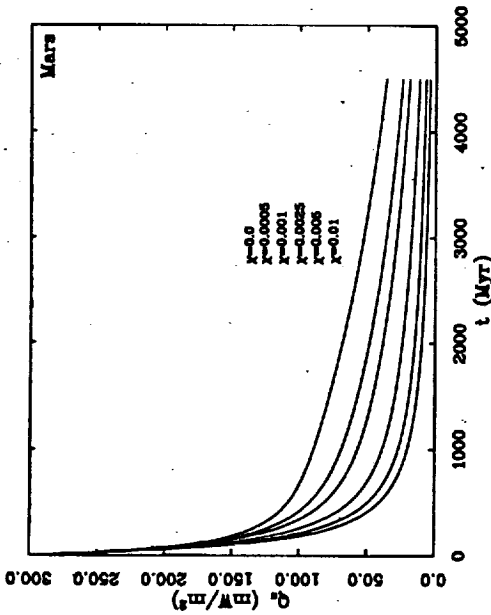
that most of the crustal growth occurs early in the evolution of Mars, i.e., within several 100 Myr of the end of accretion. This is in accord with the evidence discussed earlier of an age ≥ 4 Gyr for the southern crustal highlands. The present mean crustal thickness depends on the choice of the crustal fractionation parameter χ. The volumetric flux of volcanics is given in Fig. 12. For a small crustal fractionation parameter ($\chi = 0.0005$) the volcanic flux decreases rapidly early in the evolution, but it continues throughout the history of the planet. For larger values of the parameter χ, the interior is completely depleted and the volcanic flux drops to low levels.

With the extraction of the heat producing elements the lithosphere becomes considerably thicker (Fig. 13) and the mantle heat flux is reduced (Fig. 14). The heat flux given in Fig. 14 is the heat flux into the base of the Martian crust. The expansion and contraction of the planet is given in Fig. 15. With no crustal extraction ($\chi = 0$), only thermal contraction occurs. As the rate of crustal extraction is increased (increasing χ), the initial expansion due to crustal formation increases and the rate of thermal contraction also increases.

We can estimate the value of the crustal fractionation parameter for the Earth. It is the ratio of the crustal fractionation time $V/\dot{V}_c$ to the characteristic mantle turnover time R/u ($\dot{V}_c$ is the volumetric fractionation rate of the mantle and V_c is the volume of the mantle). Taking the rate of formation of oceanic crust to be 2.8 km² yr⁻¹ and the depth processed to be 60 km, we have $\dot{V}_c = 168$ km³ yr⁻¹. With $V_c = 10^{12}$ km³, we find that the characteristic time for creation of the oceanic crust is $V_c/\dot{V}_c = 6$ Gyr. With $R = 5800$ km (approximately twice the mantle thickness) and $u = 0.1$ m yr⁻¹, we find that

the characteristic mantle turnover time is $R/u = 58$ Myr. Thus we find that χ is about 0.01 for the Earth at the present time.

The crustal thickness on Mars has been estimated using gravity data and the assumption of Airy isostasy. For Hellas Planitia, as noted above, Sjogren and Wimberly (1981) estimated that the depth of compensation is 130 km. Using similar data and assumptions for the crater Antoniadi, Sjogren and Ritke (1982) found that the depth of compensation is 115 km. From gravity profiles across the highland-lowland escarpment, Janle (1983) found that the depth of compensation is also 115 km. Taking the crustal thickness to be $D_c = 120$ km, we find from Fig. 11 that the corresponding crustal fractionation factor is $\chi = 0.003$, about a factor of 3 less than for the Earth. This estimate of χ is uncertain because of the poorly constrained value of the mean crustal thickness on Mars.

Accepting, for purposes of discussion, that the crustal fractionation factor for Mars is $\chi = 0.003$, we can determine rates of crustal addition from Figs. 11 and 12. The average amount of crust added in the last 1 Gyr was 600 m, that added between 1 and 2 Gyr ago was 1.8 km, and that added between 2 and 3 Gyr ago was 2.9 km. The volumetric rate of crustal magmatism was much higher early in the evolution of Mars. The decline to the lower values of crustal production rate characteristic of most of Martian geologic history occurred with about a 100 Myr time scale.

The most recent volcanism on Mars during the Upper Amazonian period (Tanaka 1986) occurred in the Arcadia, Olympus Mons, Medusae Fossae and Tharsis Montes Formations, but the principal volcanics are flood basalts in the southern Elysium Planitia. These have an area of 10^5 km^2, but Tanaka (1986) suggests that the thickness is only a few 10 m. Taking a thickness of 50 m, this is only 0.03 m when averaged over the surface of Mars.

Greeley (1987) has estimated that 26×10^6 km^3 of volcanics erupted during the Middle and Upper Amazonian. This corresponds to a mean thickness of 200 m when averaged over the entire surface of Mars. From the estimate of cratering rates given by Hartmann et al. (1981), the Upper Amazonian extended from 0 to 0.7 Gyr ago and the Middle Amazonian from 0.7 to 2.3 Gyr ago. Thus, the volume of young volcanics on Mars is broadly consistent with the model results above as volcanism represents only a part of crustal addition. It should be emphasized, however, that there are considerable uncertainties in the absolute ages and in the crustal fractionation parameter.

Other predictions of our calculations using $\chi = 0.003$ are a lithospheric thickness $D_L = 400$ km and a net global contraction corresponding to $\delta R/R = -0.001$. From Fig. 15 we see that a global expansion of $\delta R = 10$ km occurred in the first 200 Myr of the evolution of Mars. This expansion was caused by the density change associated with the generation of the early crust. For the remainder of the evolution of Mars, a nearly steady contraction occurred associated with the cooling of the interior. The total contraction sub-

Fig. 14. Dependence of the mantle heat flux Q_s on time t for different values of the crustal fractionation parameter χ.

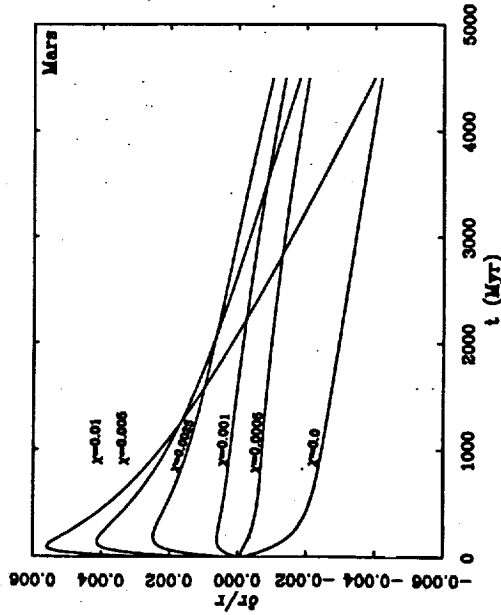

Fig. 15. Radial expansion (contraction) $\delta R/R$ as a function of time t for several values of the crustal fractionation parameter χ.

sequent to the period of early crustal differentiation was $\delta R = -13$ km. All models in Fig. 15 with substantial crustal fractionation show an early period of planetary expansion followed by a larger amount of planetary contraction.

As noted earlier, large-scale surface tectonic features of Mars include both extensional and compressional structures. The graben systems in and near the Tharsis region are likely to be the result of stresses generated by the Tharsis load. Compressive wrinkle ridges occur commonly throughout ancient terrains. These can be attributed to the early phase of rapid thermal contraction illustrated in Fig. 15.

Models of the response of Mars to the long-wavelength topographic load of the Tharsis Rise provide a reasonable fit to the observed gravity if the elastic lithosphere of Mars was globally in the range 100 to 400 km when the Tharsis construct formed (Banerdt et al. 1982; Willemann and Turcotte 1982). As the elastic lithosphere is generally ~1/2 the thickness of the thermal lithosphere, these values are consistent with those given in Fig. 13. All the models in Fig. 13 with large lithosphere thicknesses show substantial depletion in mantle radioactivity due to crustal differentiation. For no crustal differentiation, the lithosphere thickness from Fig. 13 is ~ 100 km, in agreement with the result previously obtained in Fig. 5.

V. PATTERNS OF MANTLE CONVECTION

Numerical calculations of fully three-dimensional convection in a spherical shell were recently carried out by Schubert et al. (1990) to simulate possible convective planforms in the Martian mantle. These results have important implications for proposed convective origins for major geologic features on Mars, such as the crustal dichotomy. The reader is referred to that work for more detailed information about the calculations than can be provided here.

The spherical shell model of the Martian mantle consists of a Boussinesq fluid that is heated both internally and from below to account for secular cooling, radiogenic heating and heat flow from the core. The lower boundary of the shell is assumed to be isothermal and stress-free, as appropriate to the interface between the mantle and a liquid outer core. The upper boundary of the shell is rigid and isothermal, as appropriate to the base of a thick, immobile lithosphere. The ratio of the inner radius of the shell to its outer radius is 0.55, in accordance with possible core radii in Mars. We present results for two different modes of heating. In one case, 20% of the surface heat flow originates in the core, and in the other case the percentage of heating from below is 94%. The Rayleigh numbers of both cases are approximately 100 times the critical Rayleigh numbers that characterize the onset of convection in the constant-viscosity spherical shells. These Rayleigh numbers may be an order of magnitude or more smaller than the Rayleigh number of the Martian mantle. However, the Rayleigh number of the Martian mantle is unknown
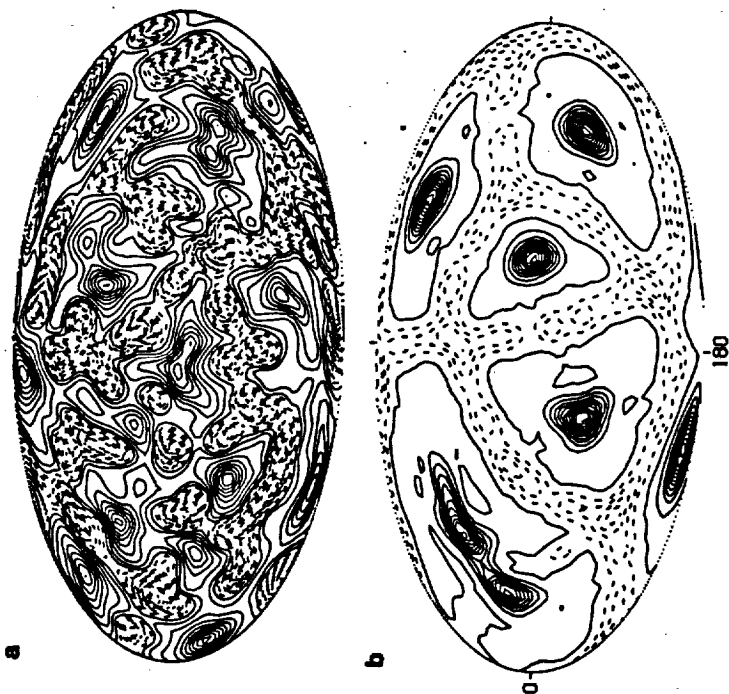
because of uncertainties in the thickness of the mantle and its material properties, viscosity in particular. The numerical approach is described in detail in Glatzmaier (1988) and Bercovici et al. (1989a). Table III lists the parameter values for the calculations discussed here.

The horizontal planforms of convection for both modes of heating are illustrated in Fig. 16 by contours of radial velocity on spherical surfaces midway through the shells. Meridional cross sections of entropy contours (equivalent to isotherms in these Boussinesq calculations) for both heating modes are shown in Fig. 17. The prominent form of upwelling in the Martian mantle is the cylindrical plume. The number of upwelling plumes is strongly influenced by the mode of heating; with only 20% heating from below, there are a dozen plumes, while 94% bottom heating produces only 6 plumes. There are fewer, stronger plumes as the proportion of bottom heating increases. Plumes carry the heat flow from the core and arise from instability of the lower thermal boundary layer at the core-mantle interface. In general, the fraction of mantle heating delivered from the core has probably decreased with time as the core cooled to temperatures not much greater than those of the lower mantle (see, e.g., Fig. 6). The isotherm cross sections of Fig. 17 show several plumes originating in the lower thermal boundary layer. Convective downwelling occurs in planar sheets that form an interconnected network surrounding the upwelling plumes. The downwellings also show cylindrical concentrations along the sheets and even distinct cylindrical downwellings.

The patterns of Fig. 16 have evolved through many overturns of the mantle and the solutions appear to be fundamentally time dependent. However, the basic nature of the convective planform, i.e., cylindrical upwelling plumes surrounded by planar downwelling sheets, does not change with time. Thus, we can expect major volcanic provinces on Mars, like Tharsis and Elysium, to reflect the cylindrical nature of upwelling mantle plumes, similar

TABLE III

Parameter Values for Three-Dimensional Spherical Convection Models of the Martian Mantle

Outer radius	3200 km
Inner radius	1762 km
Density	3450 kg m^{-3}
Core mass	1490 × 10^{20} kg
Kinematic viscosity	10^{18} m^2 s^{-1}
Thermal diffusivity	10^{-6} m^2 s^{-1}
Specific heat at constant pressure	1.2 kJ kg^{-1} K^{-1}
Thermal expansivity	2 × 10^{-5} K^{-1}
Temperature difference across the mantle	800 K
Internal heating rate (94% from below)	1.5 × 10^{-12} W kg^{-1}
Internal heating rate (20% from below)	5.3 × 10^{-12} W kg^{-1}

G. SCHUBERT ET AL.

Fig. 16. Contours of radial velocity at mid-depth in the Martian mantle in numerical models of three-dimensional mantle convection with (a) 20% and (b) 94% heating from below. The projection is an equal-area projection extending 360° in longitude and over all latitudes. Model parameter values are listed in Table III (figure after Schubert et al. 1990). Solid contours indicate radially outward motion, dashed contours denote radially inward motion.

Fig. 17. Meridional cross sections of temperature in the numerical models of Fig. 13 for (a) 20% and (b) 94% heating from below.

to hot spots on the Earth. There are no sheet-like upwelling features in the Martian mantle to produce a pattern similar to the linear global system of mid-ocean ridges on the Earth. Even the mid-ocean ridges on the Earth are not connected to deep sheet-like upwellings in the Earth's mantle (Bercovici et al. 1989b). The deep upwellings in models of convection in the Earth's mantle are also cylindrical plumes. The Earth's mid-ocean ridges are shallow, passive upwellings occurring in response to the tearing of lithospheric plates by the pull of descending slabs (Bercovici et al. 1989b). The non-Newtonian rheology of the Earth's lithosphere is essential for the occurrence of plate tectonics. Mars is a one-plate planet with a thick lithosphere (Solomon 1978; Schubert et al. 1979) beneath which mantle upwellings are in the form of cylindrical plumes.

The results of the spherical convection models have implications for proposed explanations of the crustal dichotomy and the concentrations of volcanism at Tharsis and Elysium. If the crustal dichotomy was caused by a
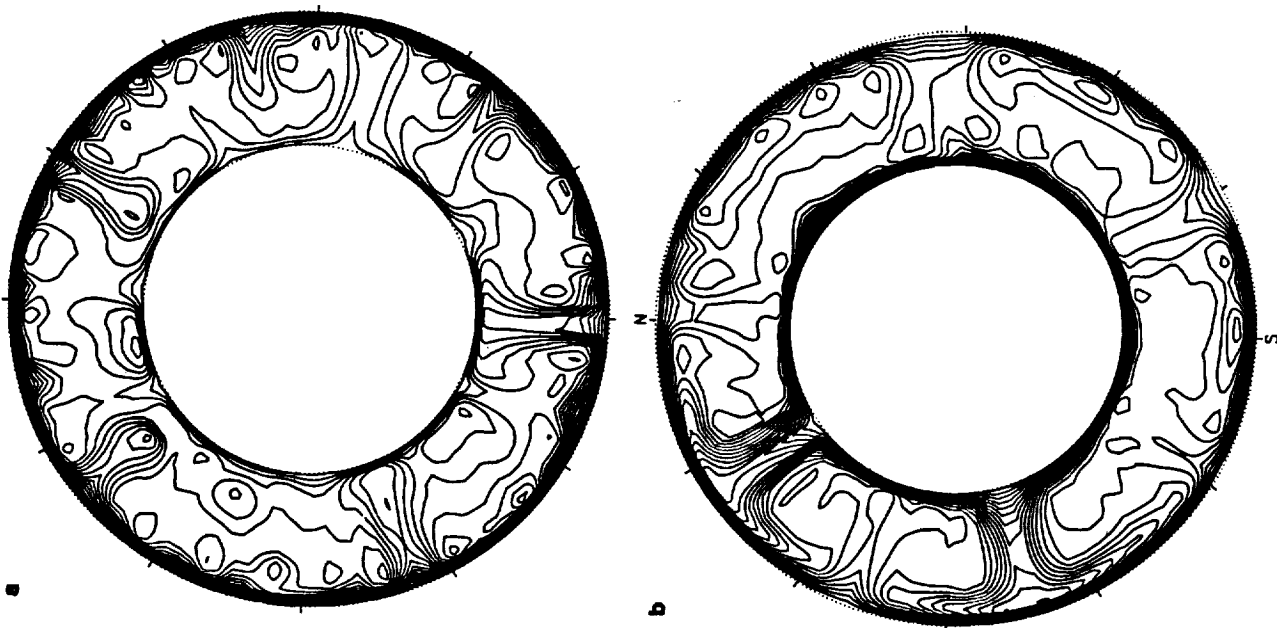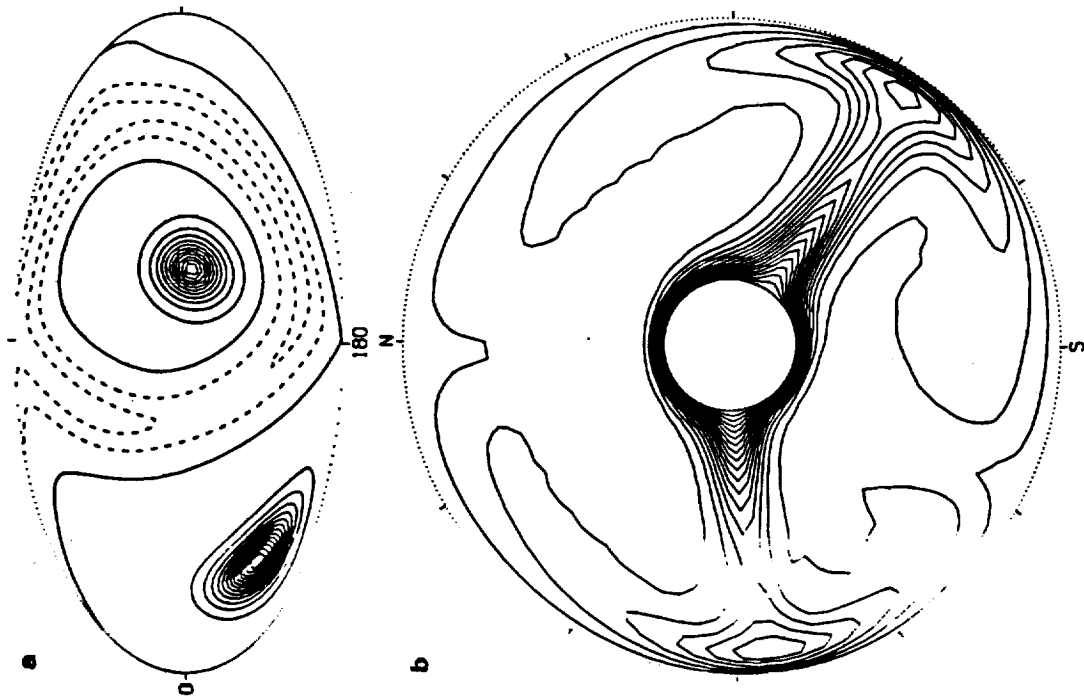
Fig. 18. (a) and (b) are similar to Figs. 16 and 17 but for a small Martian core of radius 0.2 times the radius of Mars. In the model 90% of the heating is from below.

convective system dominated by spherical harmonic degree $\ell = 1$ (Schubert and Lingenfelter 1973; Lingenfelter and Schubert 1973; Wise et al. 1979a) with upwelling under the northern hemisphere, then the convection must have been driven strongly from below (while our models produced 6 to 12 plumes, the number of plumes decreases with increasing percentage of bottom heating). Such strong heating concentrated deep within Mars can arise from the heating pulse accompanying core formation or from the flow of heat from a hot core. Indeed, the overturning accompanying core formation could in itself be an $\ell = 1$ mode (Stevenson 1980), obviating the need for a thermally driven motion.

Core size is another important factor in determining the number of convective plumes. With smaller cores there is a tendency toward fewer upwelling plumes (Zebib et al. 1983). This is confirmed by the results of Fig. 18, which shows mid-depth radial velocity contours and isotherms in meridional cross section in the mantle of a Mars model with a core radius of 0.2 times the radius of Mars (Schubert et al. 1990). The model has settled into a predominantly $\ell = 2$ (not $\ell = 1$, however) convection pattern. During the early stages of core formation, the effective core radius would have been smaller than the radius at present, favoring a thermally forced convection with perhaps just one dominant upwelling. Since the Martian core formed contemporaneously with accretion or within a few 100 Myr of the end of accretion, conditions favoring $\ell = 1$ convection, i.e., a small core and a deep heat source, occur very early in the evolution of Mars. If a convective mechanism is responsible for the crustal dichotomy, then the dichotomy must also be a very ancient feature.

It is not obvious from the models why there should be only two major volcanic centers (Tharsis and Elysium) on Mars. The models predict several to ~ 10 major mantle plumes. Perhaps the models are not realistic enough to predict the actual number of major hot spots on Mars. On the other hand, there may be many plumes in the Martian mantle, but the properties of the lithosphere may select only one or two of them for prominent surface expression. Plume activity could be focused beneath Tharsis if fracturing or thinning of the lithosphere in this region has facilitated magma and heat transport across the lithosphere. The temperature dependence of mantle viscosity will strongly influence the structure of plumes and their number, through the control that variable viscosity exerts on the nature and vigor of small-scale convective activity in the lower thermal boundary layer (Olson et al. 1987).

The numerical solutions discussed above can be used to infer that several km of dynamic topography could be associated with plumes in the Martian mantle (Schubert et al. 1990). Dynamic uplift is insufficient to account for the 10 km of topography in the Tharsis region. This large topographic excess must be largely the result of other processes, such as volcanic construction, magmatic thickening of the crust, or depletion of the underlying mantle (see, e.g., Sleep and Phillips 1979,1985; Solomon and Head 1982). Nevertheless,

it is likely that the Tharsis Rise and its volcanic constructs are a consequence of a strong mantle plume (or grouping of plumes) beneath the region.

VI. CONCLUSIONS

Several themes emerge from this overview of the thermal history of Mars. The first is the hot initial state of the planetary interior and the sharp contrasts that can be drawn between the first 1 Gyr of Martian history and the subsequent 3.5 Gyr. As a result of accretional heating and core formation essentially contemporaneous with planetary formation, the early history of Mars was characterized by high internal temperatures, a vigorously convecting mantle, and high surface fluxes of heat and magma. Outgassing contributed to an early atmosphere, and widespread magmatism may have helped trigger the release of subsurface water and large-scale floods. Parameterized convection models indicate, however, that on a time scale of only a few 100 Myr the mantle convective engine slowed, as primordial interior heat was lost and as radioactive heat production decayed or was concentrated into the shallow crust. Rapid interior cooling led to a globally thick lithosphere and was accompanied by global contraction, recorded in the pervasive formation of wrinkle ridges now preserved on ancient geologic units. The last 3.5 Gyr of Martian history was marked, in contrast, by slow cooling and by the concentration of volcanic and tectonic activity in ever more limited regions.

The second theme of Martian thermal history is the strong role of plumes expected for mantle convection. As long as a significant fraction of mantle heating comes from the core, three-dimensional convection calculations indicate that plumes dominate the upwelling portions of the flow. At least some of those plumes would be expected to have strong signatures in the surface topography and volcanic flux. The Tharsis and Elysium volcanic provinces are probably the consequences of plume-delivered heat and magma. The number and characteristics of plumes depend on the relative contributions of radioactivity and core cooling to the mantle heat budget, as well as the size of the core. While current models do not predict as few as 2 dominant plumes or plume families, development of Tharsis and Elysium very early in Martian history, when core cooling occurred at its highest rate, is favored.

A third theme of this overview is the dominating influence of core sulfur concentration on the thermal evolution of the core and the history of the Martian magnetic field. A core with more than ~ 15 wt % S probably would not crystallize a solid inner core and probably would not be thermally convecting at present. This critical S concentration is tantalizingly close to estimates of the core sulfur content from elemental abundances of SNC meteorites. Therefore, a nearly completely fluid core that is nonconvecting or only weakly thermally or chemically convecting may provide an explanation for the lack of a present Martian magnetic field or the existence of a very weak one.

A final theme of this overview is the strong impact that new information from Mars would have on our understanding of the origin and thermal evolution of the planet. Detection of an internal magnetic field or evidence for a paleofield would strongly constrain the evolution of the Martian core. Seismic determination of the thickness of the crust would provide a crucial tie point to discussions of the planetary magmatic budget, and a seismic estimate of the radius and state of the core would enable a considerably more confident assessment of bulk composition. Measurement of surface heat flow would substantially constrain the present mantle heat production. Finally, the return of Martian igneous rocks to terrestrial laboratories would provide crucial knowledge of the detailed absolute time scale for the major events in the history of the planet.

Geoid, Topography, and Convection-Driven Crustal Deformation on Venus;

Mark Simons, Bradford H. Hager, and Sean C. Solomon, Department of Earth, Atmospheric, and Planetary Sciences, Massachusetts Institute of Technology, Cambridge, MA 02139.

Introduction. High-resolution Magellan images and altimetry of Venus reveal a wide range of styles and scales of surface deformation [1] that cannot readily be explained within the classical terrestrial plate tectonic paradigm. The high correlation of long-wavelength topography and gravity and the large apparent depths of compensation suggest that Venus lacks an upper-mantle low-viscosity zone [2-5]. A key difference between Earth and Venus may be the degree of coupling between the convecting mantle and the overlying lithosphere. Mantle flow should then have recognizable signatures in the relationships between surface topography, crustal deformation, and the observed gravity field [6,7].

Model. We explore the effects of this coupling by means of a finite element modelling technique. The crust and mantle in these models are treated as viscous fluids. We solve both the equations of motion and the heat equation at every time step using a modified version of the 2-D Cartesian finite-element program ConMan [8]. A passive marker chain tracks the crust-mantle interface and permits variation in the crustal buoyancy as well as specific crustal and mantle rheologies. These rheologies depend on composition, temperature and stress. In addition to the flow field, the stress field in the lithosphere, the surface topography, and the resulting geoid are readily calculated. The models presented here use an irregular finite-element mesh that is 50 elements high and 160 elements wide. Our maximum resolution is in the 40-km-thick top layer, where each element is 2 km high and 5 km wide. In all, the mesh is 800 km in the horizontal dimension and 400 km in the vertical dimension. We impose free-slip boundary conditions on the top and side walls, with no flow through these walls. Flow at the bottom boundary is constrained to be vertical with no horizontal flow permitted. This last boundary condition gives a virtual 800 km by 800 km box. The surface topography is calculated from the vertical stresses on the top wall of the box. Top and bottom temperatures are fixed at 500°C and 1250°C, respectively. Initially, we impose a linear temperature gradient across the lithosphere and set the rest of the mantle to be isothermal. We investigate two classes of models. Flow in the first class is initiated with a sinusoidal temperature perturbation throughout the box. This results in mantle flow that is dominated by concentrated downwelling (Figure 1b). In the second class of models, flow is driven by a hot patch at the side of the box, thereby driving flow by concentrated upwelling (Figure 1a).
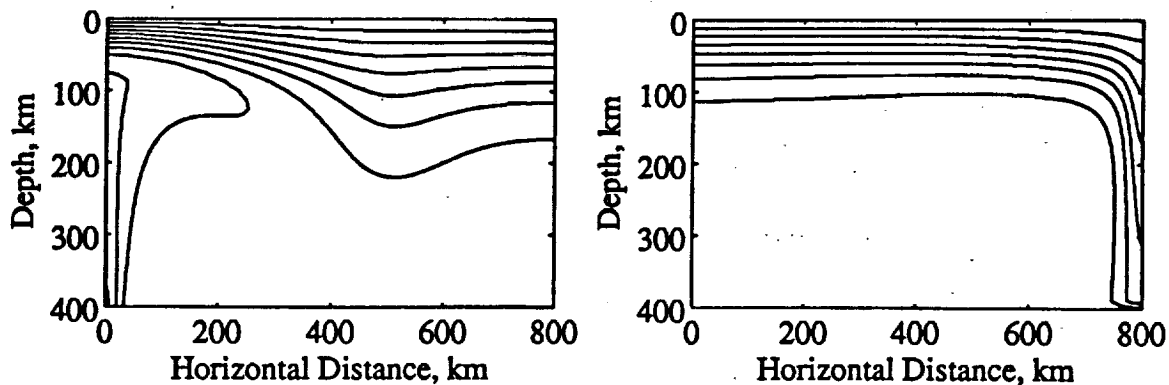

Figure 1. Temperature contours at 130 My for the (a) upwelling and (b) downwelling models. Contour interval is 100 °C; the top of the box is at 500 °C.

Results. In all our models, convection produces horizontal compressional stresses in lithosphere above downwelling mantle and extensional stresses in lithosphere above upwelling mantle. As the convective vigor increases so does the magnitude of the stress. In models with constant-viscosity mantle overlain by a constant-viscosity crust, stress in the crust reaches values in excess of 100 MPa in less than 100 My. We find that the rate of increase in compressive stress decreases with increasing crustal viscosity. This is because the stronger the crust, the more the development of the convective instability in the mantle driving the deformation is impeded. We also find that the magnitude of the peak compressive stress achieved above the downwelling increases with higher viscosities and/or with thinner initial crustal layers; the stronger the crustal lid, the more are tractions from mantle convection supported in the crust. Since force balance on the crust requires that shear traction integrated along the base be balanced by normal tractions integrated through its thickness, the thinner the crust, the larger the horizontal stresses.

Both analytical models [9,10] and our numerical models of convection-induced crustal flow indicate that the amplitude and sign of the topography are highly time- and rheology-dependent. In general, possible responses of the crust to mantle flow can be divided into three categories. The first involves little, if any, crustal flow, and topography results mainly from the transmission of normal tractions induced by density contrasts within the mantle. The second possible regime involves substantial crustal flow, with geologically rapid thickening over convective downwelling and thinning over convective upwelling. In this regime the effects of crustal thickness variations dominate the topography. A third possible regime lies between the first two, with "in phase" deformation on short time scales and crustal flow on longer time scales. A strong mantle lithosphere tends to shield the crust from convective shear tractions, and topography results mainly from the transmission of convective normal tractions. A relatively weak lower crust facilitates crustal deformation, and the isostatic effects of crustal thickness variations dominate the topography.

Consideration of geoid to topography ratios (GTRs) can restrict which regime of crustal response is appropriate for Venus. The distibution of estimated GTRs for several highland regions on Venus is bimodal with two clusters around 10 and 25 m/km [5]. The positive correlation of long-wavelength gravity and topography implies that there are no major regions that have negative GTRs. To keep the GTRs positive, the geoid must follow the surface topogaphy in sign at all times. Although the regime of negligible crustal flow can correctly predict both the sign and magnitude of the GTRs, it does not allow for the crustal deformation (i.e., flow) inferred from observations of tectonic features on Venus.

In contrast to the regime of negligible flow, that of time-dependent crustal flow generates topography that changes sign. Over a mantle downwelling, the topography is negative in the early stages of deformation and positive in the later stages of deformation; the converse holds over a mantle upwelling. During the transitional period the topography goes through zero, the geoid does not go through zero, and the GTR is unbounded; this singularity is not observed on Venus. An example of the evolution of the GTR for a model in the time-dependent regime is shown in Figure 2. Note that before 90 My both topography and geoid are negative, but at 90 My crustal thickening effects begin to dominate and the topography switches sign, causing the GTRs to first become unbounded and then negative.

In the absence of a mechanism by which the sign of the geoid anomaly mimics that of the topography over a given upwelling or downwelling, only the regime of rapid crustal flow is

plausible. In the case of mantle downwelling this would also require that the lower mantle be more viscous than the upper mantle in order to produce the required positive geoid anomalies. This has already been shown to be true for the Earth, where the observed geoid highs over regions of mantle upwelling and regions of mantle downwelling are best explained by the presence of a strong lower mantle [11,12]. The large positive GTRs and the presence of large shield volcanoes in certain highland regions on Venus, such as Beta Regio and Eistla Regio, are best explained as areas of mantle upwelling [5,13,14]. The regime of rapid crustal flow predicts crustal thinning over the upwelling. However, the extensive partial melt and ensuing volcanism expected over such regions of mantle may outweigh the effects of crustal thinning on the surface topography and thus also yield postive GTRs [15].
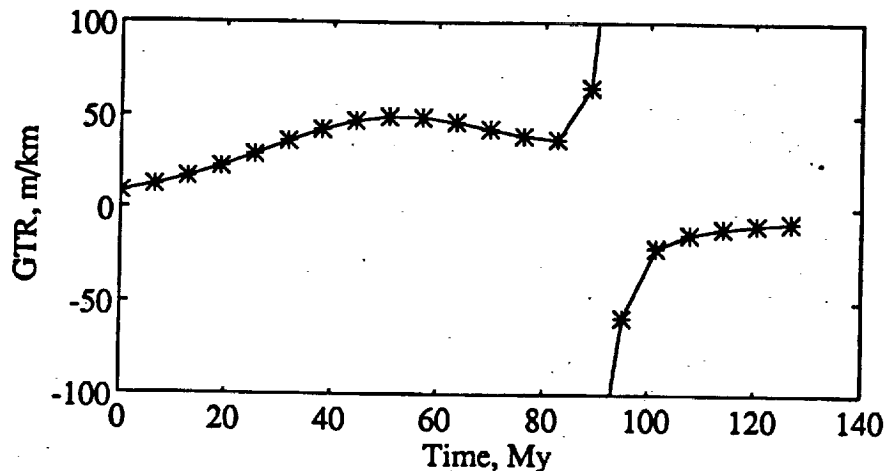
Figure 2. Evolution of GTR with time. At each time step, the GTR shown is the slope of the best fit line to the collection of geoid and topography values upward continued to 250 km above the surface nodes in the model. The result is for a downwelling model, with a crust of constant viscosity 50 times that of the mantle. In this model the sign of the topography is time-dependent, but that of the geoid is not. The singularity at about 90 My corresponds to the time when topography crosses the zero datum. Note that the GTRs for this model are neither always positive nor always bounded.

References: [1] S. C. Solomon et al., Science, 252, 297, 1991; [2] W. S. Kiefer et al., Geophys. Res. Lett., 13, 14, 1986; [3] B. G. Bills et al., J. Geophys. Res., 92, 10, 1987; [4] R. J. Phillips et al., Science, 252, 651, 1991; [5] S. E. Smrekar and R. J. Phillips, Earth Planet. Sci. Lett., 107, 587, 1991; [6] R. J. Phillips, Geophys. Res. Lett., 13, 1141, 1986; [7] R. J. Phillips, J. Geophys. Res., 95, 1301, 1990; [8] S. D. King et al., Phys. Earth Planet. Inter., 59, 195, 1990; [9] D. L. Bindschadler and E. M. Parmentier, J. Geophys. Res , 95, 21, 1990; [10] H. Schmeling and G. Marquart, Geophys. Res. Lett , 17, 2417, 1990; [11] M. A. Richards and B. H. Hager, J. Geophys. Res , 89, 5987, 1984; [12] B. H. Hager, J. Geophys. Res , 89, 6003, 1984; [13] R. E. Grimm and R. J. Phillips, J. Geophys. Res., 96, 8305, 1991; [14] R. E. Grimm and R. J. Phillips, J. Geophys. Res , in press, 1991; [15] R. J. Phillips et al., Science, 252, 651, 1991.

Geoid, Topography, and Convection-Driven Crustal Deformation on Venus;

Mark Simons[1], Bradford H. Hager[1], and Sean C. Solomon[2], [1]Department of Earth, Atmospheric, and Planetary Sciences, Massachusetts Institute of Technology, Cambridge, MA 02139, [2]Department of Terrestrial Magnetism, Carnegie Institution of Washington, Washington, DC 20015.

Introduction. High-resolution Magellan images and altimetry of Venus reveal a wide range of styles and scales of surface deformation [1] that cannot readily be explained within the classical terrestrial plate tectonic paradigm. The high correlation of long-wavelength topography and gravity and the large apparent depths of compensation suggest that Venus lacks an upper-mantle low-viscosity zone [2-5]. A key difference between Earth and Venus may be the degree of coupling between the convecting mantle and the overlying lithosphere. Mantle flow should then have recognizable signatures in the relationships between the observed surface topography, crustal deformation, and the gravity field [6,7]. Therefore, comparison of model results with observational data can help to constrain such parameters as crustal and thermal boundary layer thicknesses as well as the character of mantle flow below different Venusian features. We explore in this paper the effects of this coupling by means of a finite element modelling technique.

Model. The crust and mantle in the models are treated as viscous fluids. We solve both the equations of motion and the heat equation at each time step using a modified version of the two-dimensional, Cartesian finite-element program ConMan [8]. Our formulation assigns material properties to each element and explicitly tracks the free surface topography and the crust-mantle interface by letting the grid deform with time in a semi-Lagrangian fashion. This procedure permits variation in the crustal buoyancy as well as specific crustal and mantle rheologies that can depend on composition, temperature and stress. In addition to the flow field, the stress field in the lithosphere, the surface topography, and the resulting geoid are readily calculated. The model domain is a square box. We impose free-slip boundary conditions on the bottom and side walls, with no flow through these walls. The top of the box is a true free surface, so there is no need to derive surface topography from vertical stresses on the top of the box. We investigate two classes of models. In the first class flow is dominated by concentrated upwelling (Figure 1a), and in the second class flow is dominated by concentrated downwelling (Figure 1b). We vary the initial crustal and thermal boundary layer thicknesses as well as the effect of crustal and mantle viscosities that are either constant, temperature-dependent, or fully non-Newtonian.

Results. In all of our models, convection produces horizontal compressional stresses in lithosphere above downwelling mantle and extensional stresses in lithosphere above upwelling mantle. As the convective vigor increases so does the magnitude of the stress. In models with constant-viscosity mantle overlain by a constant-viscosity crust, stress in the crust reaches values in excess of 100 MPa in less than 100 My. We find that the rate of increase in compressive stress decreases with increasing crustal viscosity. This is because the stronger the crust, the more the development of the convective instability in the mantle driving the deformation is impeded. We also find that the magnitude of the peak compressive stress achieved above the downwelling increases with higher viscosities and/or with thinner initial crustal layers; the stronger the crustal lid, the more are tractions from mantle convection supported in the crust. Since force balance on the crust requires that shear tractions integrated along the base be balanced by normal tractions integrated through its thickness, the thinner the crust, the larger the horizontal stresses.

Both analytical models [9,10] and our numerical models of convection-induced crustal flow indicate that the amplitude and sign of the topography are time- and rheology-dependent. In general, possible responses of the crust to mantle flow can be divided into three categories. The first involves little, if any, crustal flow, and topography results mainly from the transmission of normal tractions induced by density contrasts within the mantle. The second possible regime involves substantial crustal flow, with geologically rapid thickening over convective downwelling and thinning over convective upwelling. In this regime the effects of crustal thickness variations dominate the topography. A third possible regime lies between the first two, with "in phase" deformation on short time scales and crustal flow on longer time scales. A strong mantle lithosphere tends to shield the crust from convective shear tractions, and topography results mainly

from the transmission of convective normal tractions. A relatively weak lower crust facilitates crustal deformation, and the isostatic effects of crustal thickness variations dominate the topography.

Consideration of geoid-to-topography ratios (GTRs) can restrict the regime of crustal response appropriate for Venus. The distribution of estimated GTRs for several highland regions on Venus is bimodal with two clusters around 10 and 25 m/km [5]. The positive correlation of long-wavelength gravity and topography implies that there are no major regions that have negative GTRs. To keep the GTRs positive, the geoid must follow the surface topography in sign at all times. Although the regime of negligible crustal flow can correctly predict both the sign and magnitude of the GTRs, it does not account straightforwardly for the crustal deformation (i.e., flow) inferred from observations of tectonic features, and particularly areas of extensively deformed terrain, on Venus.

In contrast to the regime of negligible flow, that of time-dependent crustal flow generates topography that changes sign. Over a mantle downwelling, the topography is negative in the early stages of deformation and positive in the later stages of deformation; the converse holds over a mantle upwelling. During the transitional period the topography goes through zero, the geoid does not go through zero, and the GTR is unbounded; this singularity is not observed on Venus.

In the absence of a mechanism by which the sign of the geoid anomaly mimics that of the topography over a given upwelling or downwelling, only the regime of rapid crustal flow is plausible. In the case of mantle downwelling this would also require that the lower mantle be more viscous than the upper mantle in order to produce the required positive geoid anomalies. This layering of viscosity structure has already been shown to hold for the Earth, where the observed geoid highs over regions of mantle upwelling and regions of mantle downwelling are best explained by the presence of a strong lower mantle [11,12]. The large positive GTRs and the presence of large shield volcanoes in certain highland regions on Venus, such as Beta Regio and Eistla Regio, are best explained as areas of mantle upwelling [5,13,14]. The regime of rapid crustal flow predicts crustal thinning over the upwelling. However, the partial melting and ensuing volcanism and crustal plutonism expected over such regions may outweigh the effects of crustal thinning on the surface topography and thus also yield positive GTRs [15].

References. [1] S. C. Solomon et al., Science, 252, 297, 1991; [2] W. S. Kiefer et al., Geophys. Res. Lett., 13, 14, 1986; [3] B. G. Bills et al., J. Geophys. Res., 92, 10, 1987; [4] R. J. Phillips et al., Science, 252, 651, 1991; [5] S. E. Smrekar and R. J. Phillips, Earth Planet. Sci. Lett., 107, 587, 1991; [6] R. J. Phillips, Geophys. Res. Lett., 13, 1141, 1986; [7] R. J. Phillips, J. Geophys. Res., 95, 1301, 1990; [8] S. D. King et al., Phys. Earth Planet. Inter., 59, 195, 1990; [9] D. L. Bindschadler and E. M. Parmentier, J. Geophys. Res., 95, 21, 1990; [10] H. Schmeling and G. Marquart, Geophys. Res. Lett., 17, 2417, 1990; [11] M. A. Richards and B. H. Hager, J. Geophys. Res., 89, 5987, 1984; [12] B. H. Hager, J. Geophys. Res., 89, 6003, 1984; [13] R. E. Grimm and R. J. Phillips, J. Geophys. Res., 96, 8305, 1991; [14] R. E. Grimm and R. J. Phillips, J. Geophys. Res., 97, 16035, 1992; [15] R. J. Phillips et al., Science, 252, 651, 1991.
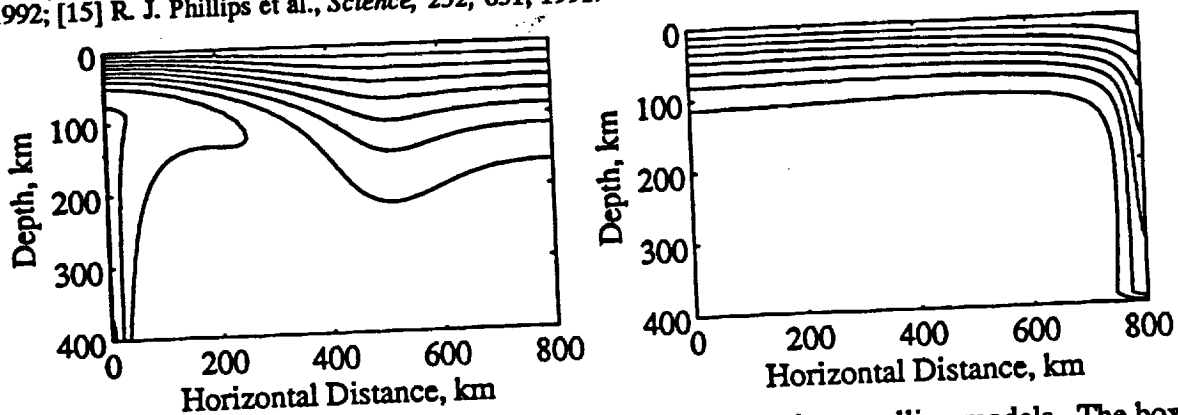

Figure 1. Temperature contours for the (a) upwelling and (b) downwelling models. The box is 800 km in the horizontal dimension and 400 km in the vertical. Top and bottom temperatures are fixed at 500 °C and 1250 °C, respectively. Contour interval is 100 °C.